ASTRONOMY & ASTROPHYSICS
SUPPLEMENT SERIES

JANUARY 1992, PAGE 365

Astron. Astrophys. Suppl. Ser. **92,** 365-399 (1992)

The Ulysses cosmic ray and solar particle investigation

J.A. Simpson[1], J.D. Anglin[2], A. Balogh[3], M. Bercovitch[2], J.M. Bouman[4], E.E. Budzinski[2], J.R. Burrows[2], R. Carvell[8], J.J. Connell[1], R. Ducros[6], P. Ferrando[6], J. Firth[2], M. Garcia-Munoz[1], J. Henrion[4], R.J. Hynds[3], B. Iwers[5], R. Jacquet[1], H. Kunow[5], G. Lentz[1], R.G. Marsden[4], R.B. McKibben[1], R. Mueller-Mellin[5], D.E. Page[7], M. Perkins[1], A. Raviart[6], T.R. Sanderson[4], H. Sierks[5], L. Treguer[6], A.J. Tuzzolino[1], K.-P. Wenzel[4] and G. Wibberenz[5]

[1] Laboratory for Astrophysics and Space Research, University of Chicago, Chicago, IL 60637, USA
[2] Herzberg Institute of Astrophysics, Natl. Research Council of Canada, Ottawa, K1A 0R6, Canada
[3] The Blackett Laboratory, Imperial College of Science and Technology, London SW7 2BZ, UK
[4] Space Science Department of ESA, ESTEC, 2200 AG Noordwijk, The Netherlands
[5] Institut für Reine und Angewandte Kernphysik, Universität Kiel, D-2300 Kiel 1, Germany
[6] Service d'Astrophysique, Centre d'Etudes Nucleaires de Saclay, 91191 Gif-sur-Yvette Cedex, France
[7] ESA at Jet Propulsion Laboratory, California Institute of Technology, Pasadena, CA 91109, USA
[8] Claredon Laboratory, Oxford University, Oxford OX1 3PU, UK

Received April 23; accepted July 25, 1991

Abstract. — The Ulysses spacecraft, launched on 6 October 1990, is the first to undertake measurements in the heliosphere far from the ecliptic plane and over the polar regions of the Sun. The instrumentation carried by the spacecraft includes a group of six charged particle telescopes to measure the energy, composition, intensity and anisotropy of nucleons in the energy range from ~ 0.5 MeV/nucleon to ~ 600 MeV/nucleon for elements in the range H to Ni. Isotopic abundances for nuclei H to Ni are obtained over a more limited energy range. Electron measurements extend from 2.5 to 6000 MeV. One set of telescopes will measure the three-dimensional anisotropies of protons and helium at low energies. A special high flux telescope provides measurements of protons and heavier particles ~ 0.2 to ~ 36 MeV with high azimuthal resolution. These instruments were prepared by an international consortium to address a wide range of scientific objectives made possible by a mission to investigate the Sun and the heliosphere in three dimensions. Our program is called "Cosmic Ray and Solar Particle Investigation" or COSPIN.

Examples of the COSPIN scientific goals include: (i) For energetic charged particles of solar origin, to determine the role of coronal magnetic fields in their acceleration and propagation and to search for the origin of the enrichment of ^{3}He and Fe nuclei observed in some solar particle events; (ii) Using galactic cosmic radiation measurements, to explore the likely reduction or elimination of solar modulation in polar regions relative to the equator, to search for the origin of the anomalous nuclear component, and to determine the nucleosynthetic origins of nuclei at lowest measurable energies; (iii) For energetic nuclei and electrons of interplanetary origin, to study the three-dimensional character of traveling shocks, CIRs and their associated charged particle acceleration, and; (iv) As a secondary scientific objective at Jupiter encounter (closest approach 8 Feb., 1992), to characterize the energetic charged particle populations during the first traversal of the dusk side of the Jovian magnetosphere and to search for the mechanism producing the ~ 10 hour "clock" variation of Jovian electrons in the interplanetary medium. In this publication we give a detailed description of the instruments, their pre-launch performance and a sampling of preliminary results based on the data so far available, extending from turn-on on day 296, 1990 through the early days of 1991. During this period a solar flare provided nuclei in the energy range ~ 0.5 to 200 MeV/nucleon which made possible the first intercalibration of the instruments over a flux range $\sim 10^7$. Observations of six solar flare energetic charged particle events are shown for nuclei. Three of these events also accelerated electrons. An observation of a ^{3}He – rich solar particle event and the measured anisotropy of protons from a flare is reported. From observations of heavy ions in the data so far available, the effectiveness of employing position-sensing semi-conductor detectors for obtaining enhanced elemental and isotopic resolution is demonstrated, even at this early stage of analysis. These preliminary results confirm that the instruments are functioning properly, and that their design has achieved both the wide dynamic range required to encompass the unexpected phenomena likely to be encountered on this exploratory and discovery mission, and the precision required to make definitive measurements on this, the only mission presently planned to explore the high latitude regions of the heliosphere.

Key words: cosmic rays — solar particles — heliosphere.

Send offprint requests to: J.A. Simpson.

1. Scientific objectives.

Investigations over the past 35 years have shown that the heliosphere is the largest structure so far directly accessible for spacecraft investigations of the electrodynamical interactions of plasmas, magnetic fields, and energetic charged particles on astrophysical scales. Studies made with the Pioneer 10 and 11, and Voyager 1 and 2 spacecraft out to > 50 A.U. have yielded discoveries vital for understanding phenomena such as collisionless shocks, charged particle acceleration mechanisms, galactic cosmic ray propagation and the interactions of the Sun with its environment mediated by the plasmas and magnetic fields in the solar wind. These phenomena, while studied locally in the heliosphere, are important in a wide variety of settings throughout the galaxy and beyond. A limitation on heliospheric investigations to date is that observations have so far been available only from ground-based and spacecraft investigations restricted to the low solar latitudes in and near the ecliptic. Very little has been established regarding phenomena in the high latitude regions of the heliosphere or indeed, in the polar regions of the Sun itself, except through remote sensing techniques such as radio scintillations and the limited observations that can be made of the polar regions of the sun as a result of the seven degree tilt of the Sun's rotation axis with respect to the ecliptic.

The Ulysses Mission is the first mission, and the only mission in the foreseeable future, that will undertake measurements in regions of the heliosphere far from the ecliptic plane and over the polar regions of the sun. The instrumentation which it carries must be capable of being both exploratory, with the wide dynamic range of instrument response required to encompass unexpected phenomena and, simultaneously, definitive, with the sophistication and resolution necessary to characterize completely whatever phenomena are discovered.

For these investigations the galactic cosmic radiation, the anomalous nuclear components, the galactic and jovian electron components, and the solar flare accelerated high energy particles are important charged particle test "probes" of large scale heliospheric phenomena and their changes with time. The measurement of a wide range of charged particle properties, including energies, anisotropies, spectra, and the chemical and isotopic composition of nucleons reveals specific acceleration mechanisms, propagation modes, and small scale transient phenomena, and provides information important for astrophysics beyond the solar system as well. These measurements, provided by the Cosmic Ray and Solar Particle Investigation (COSPIN), have a central role in achieving the scientific goals of the Ulysses Mission. For example, the COSPIN will measure at low energies (e.g., $\sim$ 1 MeV) the acceleration of charged particles from solar flares, radial and corotating interplanetary shocks and, at higher energies (e.g., $\sim 0.1 - 1$ GeV), the modulation of the galactic cosmic ray spectrum resulting from large scale interplanetary dynamical phenomena. Thus, the primary experimental goals of the COSPIN are to address fundamental astrophysical questions concerning solar, heliospheric and galactic phenomena in the hitherto unexplored high latitude regions of the Sun and heliosphere.

With Ulysses plasma and magnetic field measurements, and in collaborative investigations with Pioneer-10, Voyager -1, and Voyager-2 in the distant heliosphere, we expect to be able to deduce the large scale, three-dimensional structure of the heliosphere and to investigate its changes with solar cycle activity.

Since Ulysses will reach its maximum latitude when the $\sim$ 11 year solar cycle approaches a minimum, the modulation of cosmic rays will also be near a minimum. Thus, depending upon the topology of the heliospheric magnetic fields over the solar polar regions, we may have access to a lower energy portion of the interstellar spectrum than would be possible at low latitudes.

The following are some of the specific scientific goals of the COSPIN investigators for the Ulysses Mission during 1990-1995.

From the measurement of charged particles of solar origin we shall study their energy spectra, elemental and isotopic composition and anisotropy during propagation to high heliospheric latitudes to determine:

a) The role of coronal magnetic fields for the storage and propagation of solar flare accelerated nuclei and electrons:
b) The origin of the enrichment of ^{3}He and Fe observed in some solar flares;
c) The importance of emission of energetic particles from regions other than solar flares.

For the galactic cosmic ray investigations we shall:

a) Explore the likely reduction in solar modulation near solar minimum over the solar polar regions to deduce the interstellar galactic cosmic ray spectra at low energies both for nucleons and electrons, and to determine the abundances of electron-capture isotopes.
b) Investigate the propagation of nuclei compared to that of electrons in polar and equatorial regions during the period when nucleons are predicted to gradient drift from over the polar regions to the inner heliosphere. This would provide a test of the importance of the 22 year solar polar magnetic field reversal cycle for cosmic ray modulation.
c) Based on "b" above, search for evidence that the anomalous nuclear component may be accelerated at a terminal shock over the heliospheric polar regions;
d) Measure the elemental and isotopic abundances of the galactic cosmic rays from H to Ni down to a low energy threshold determined by either:

i) residual modulation if significant transverse magnetic field irregularities exist at polar latitudes, or; ii) instrumental response thresholds if the field lines are open to the interstellar medium so that residual modulation is unimportant;

e) From "d" above, attempt to derive the nucleosynthetic origin of the low energy interstellar cosmic radiation.

With regard to the acceleration or modulation of charged particles in the interplanetary medium, we intend to:

a) Study the latitudinal extent and three-dimensional character of interplanetary shocks which accelerate charged particles and modulate (e.g., by Forbush decreases) the galactic cosmic rays and the anomalous nuclear component;

b) Establish the latitudinal gradients of nucleons and electrons during the solar magnetic cycle prevailing in 1992-1996;

c) Measure the distribution of Jovian electrons as probes of heliospheric magnetic fields at high latitudes.

During the Ulysses encounter with Jupiter (closest approach, 8 February 1992) our magnetospheric studies will include:

a) The first traversal of the dusk side of the Jovian magnetosphere;

b) A search for the mechanism producing the $\sim$ 10 hour "clock" variation of the Jovian relativistic electron spectra both in the magnetosphere and in interplanetary space;

c) Measurements of the intensities, spectra, anisotropies, and composition of the trapped radiation.

2. The COSPIN measurements.

To achieve the scientific goals discussed above, a degree of flexibility is needed from the instrumentation which can only be realized by employing a variety of sensor designs. A set of five telescope subsystems are combined within the COSPIN experiment to cover the charged-particle flux in the energy and nuclear charge intervals shown in Figures 1 and 2. The five sensor subsystems developed for COSPIN are listed in Table 1, together with the participating institutions having prime responsibility for each subsystem. Other areas of hardware responsibility, where applicable, are also shown.

Each COSPIN sensor is designed to address a different range of the measurements required to characterize the cosmic and other energetic charged particles in the high latitude regions of the heliosphere. The High-Energy Telescope (HET) will make spectral and chemical-abundance measurements of all elements from H to Ni over an energy range of $\sim 14 - 600$ MeV/nucleon depending on nuclear charge, and isotopic measurements from H to Ni over a more limited energy range. The Low-Energy Telescope (LET) will provide spectral and chemical-abundance measurements over the charge range $Z = 1 - 26$, to carry the chemical composition downward in energy to 1.8 MeV for protons and $\sim$ 3 MeV/nucleon for particles with $Z > 5$. The twin Anisotropy Telescopes (ATs) will measure the three-dimensional anisotropies of protons and alpha particles in the energy range 0.7 to 7 MeV/nucleon. The High-Flux Telescope (HFT) will provide measurements of protons and heavier particles above 0.3 MeV/n with high immunity to electron contamination under high flux conditions and with high azimuthal resolution. The Electron Telescope (KET) is designed to measure electron fluxes between 2.5 and 6000 MeV and to determine energy spectra in the range 7-170 MeV. It will also provide proton and alpha-particle measurements over a wide energy range. A Digital Processing Unit (DPU) combines the data from all sensor subsystems into a COSPIN data format and, after suitable processing, transmits them into the spacecraft telemetry stream. Two redundant power converters complete the COSPIN package. A simplified block diagram of the COSPIN experiment and its interface to the spacecraft is shown in Figure 3.

The development of the instrumentation concepts extended from 1975 to 1978. The instrumentation was designed, built and tested for space flight for the initially-planned STS launch by NASA in 1983. Because of the long duration of the Ulysses Mission, care has gone into the design of COSPIN to assure reliability and the ability to survive, to the maximum extent possible, failures in individual subsystems. A basic ground rule is that no single failure in any subsystem should result in complete loss of useful data from COSPIN. Thus, certain critical subsystems, such as the low voltage power converter and the central processing unit (CPU) of the DPU, have been made completely redundant. The other subsystems have been designed to be isolated from each other so that a failure in one would cause a loss of data only from that subsystem.

The complete COSPIN instrumentation is packaged in five units mounted on the spacecraft platform and interconnected as shown schematically in Figure 4. According to the Ulysses Project nomenclature the units are referred to as SIM-1, SIM-2, etc., and the units are so identified in some of the illustrations and tables in this paper. A tungsten shield protects the HET telescope from the intense γ-radiation of the spacecraft Radio-isotope Thermo-electric Generator (RTG) to minimize background in key data channels. The mass, telemetry allocation, and spacecraft power consumption of the COSPIN subsystems and of the COSPIN experiment as a whole are shown in Table 2.

The Ulysses Mission overview and spacecraft trajectory have been described by Wenzel, *et al.* (1992). Key times for COSPIN measurements include:

Jupiter Encounter
(closest approach, 8 February 1992)
South Polar Pass Period > 70°S
(26 June, 1994 to 6 November, 1994)
Equatorial Passage (S to N)
(6 November, 1994 to 21 June, 1995)
North Polar Pass Period > 70°N
(21 June, 1995 to 30 September, 1995)
End of Mission
(September 1995)

Many of the studies to be undertaken by the Ulysses mission in general and the COSPIN investigation in particular are greatly strengthened by the availability of comparable measurements from a stationary point in the heliosphere to permit separation of spatial from temporal variations, and to provide a baseline against which spatial variations may be measured. A 1 A.U. baseline for the Ulysses measurements is provided by:

a) An instrument almost identical to the COSPIN HET on the Combined Release and Radiation Effects Satellite (CRRES);
b) Instruments on the IMP-8 satellite which provide measurements of the interplanetary charged particles, the solar wind, and magnetic fields;

and eventually

c) Instruments on NASA's Wind satellite, to be launched in 1993, which will take over and continue the measurements that IMP 8 provides now.

3. Initial postlaunch results.

Although the experiment data records (EDRs) were not available at the time of preparing this report, sufficient "quick look" data have been available to obtain significant results for the first approximately 70 days of the mission. The Sun was extremely cooperative in producing a series of six solar flares (labelled a-f in Fig. 5) which accelerated protons, heavier nuclei and electrons. Figure 5 illustrates measurements of one hour averages of counts per second for protons over a wide range of energy intervals for the six (6) solar flare events in this period. Figure 6 is the corresponding set of electron measurements during the same period.

Figure 7 is the proton differential energy spectrum of the solar flare event in progress at the time COSPIN power was first turned on at 1643 UT on Day 296 (23 October), 1990. The spectrum covers an energy range extending from $\sim$ 0.5 MeV to $\sim$ 200 MeV and a dynamic flux range of seven (7) orders of magnitude. The spectrum in Figure 7 is a power law, $E^{-2.7}$, above $\sim$ 2 MeV but it flattens at lower energies. This spectrum is a composite of measurements from all 6 independent COSPIN charged particle telescopes, each calibrated in particle beams independently before launch and each possessing different geometrical factors. The measurements in Figure 7 have provided the first direct test of the intercalibration of these telescopes. It is clear that these independent determinations of geometrical factor, efficiencies of detection, energy thresholds, etc., for the COSPIN instruments are remarkably consistent.

In the following sections we describe in detail the individual components of the COSPIN instrumentation, and also present some of the first post-launch results which have been obtained with each instrument to demonstrate the capabilities of the instrumentation. The following instrument descriptions extend and complement descriptions provided earlier by Simpson *et al.* (1983).

4. The COSPIN instrumentation.

4.1. The low energy telescope (LET).

The COSPIN Low Energy Telescope (LET) measures the flux, energy spectra and elemental composition of solar energetic particles and low energy cosmic ray nuclei from hydrogen up to iron. The instrument covers an energy range from $\sim$ 1 to $\sim$ 75 MeV/n, using a double dE/dX vs. E telescope. Comprehensive on-board particle identifier electronics and an event priority system enable rare nuclei to be analyzed in preference to the more common species. Isotope separation for light nuclei such as He is also achieved.

As shown in the photograph of SIM 1 in Figure 8, the LET sensor and associated analogue and digital electronics are mounted in the central portion of the SIM-1 package, between the Anisotropy Telescopes (cf. Sect. 4.2) and the Digital Processing Unit (cf. Sect. 4.6). The instrument aperture is protected by a hinged cover that was opened by telecommand after launch. A gas purge system was also included to provide additional protection against detector contamination during ground testing and the ascent phase of the launch.

The LET sensor consists of a four-element solid-state detector telescope surrounded by a cylindrical plastic scintillator anticoincidence shield, together with associated analogue electronics. The telescope is shown in schematic form in Figure 9. Detectors D_1 and D_2 are large-area (6 cm^2) surface barrier devices having nominal thicknesses of 30 microns (D_1) and 100 microns (D_2), while D_3 and D_4 are 2000 micron-thick Li-drifted devices of 10.0 and 12.5 cm^2 active area, respectively. D_4 forms part of the anticoincidence shield. Relevant physical parameters for the detectors used in the flight sensor are given in Table 3. The aperture of the telescope is covered by two thin foils, an inner Ti foil (2 microns) and an outer Kapton foil (8 microns), included for electrical screening and thermal control purposes, respectively. The telescope geometrical factor, defined by two circular collimators mounted in front of D_1 and D_2 in order to reduce unwanted edge effects, has a value of 0.58 cm^2 sr for the coincidence

channels. Low resolution single-detector only) measurements of protons and alpha particles are also made. In this case, the geometrical factor is ~ 9.1 cm^{2}sr.

The signals from detectors D_1, D_2 and D_3 are fed into individual amplifier chains consisting of a charge-sensitive preamplifier followed by a parallel combination of three pulse-shaping voltage amplifiers (PSA). To accommodate the large dynamic range required, separate low-and high-gain PSA have been used, selected via an analogue switch controlled by the third (fast) PSA in conjunction with a discriminator. The selected outputs are fed into a common 10-bit (1024 channel) ADC that provides pulse height information. The fast PSA are followed by a number of threshold discriminators, the outputs of which are used in the coincidence logic to define a series of counting rate channels.

In addition, the outputs of the slower PSA are fed into a Particle Identifier (PI) circuit that provides both counting rate and event priority information. The LET PI circuit makes it possible to obtain the counting rates corresponding to groups of nuclear species, and comprises a set of analogue function generators and discriminators that divide the instrument response into regions of different nuclear charge. The actual analogue functions used are of two types, namely

$$E_1 + b_i E_2 = a_i \quad (1)$$

and

$$E_2 (b_i + E_3) = a_i \quad (2)$$

where E_1, E_2 and E_3 are the energies deposited in detectors D_1, D_2 and D_3, respectively, and a_i, b_i are constants. For particles stopping in D_2, the loci of points satisfying equation (1) for given pairs of (a_i, b_i) values define boundaries on the $\Delta E\,(\equiv E_1)$ vs. residual $E\,(\equiv E_2)$ diagram that separate the tracks corresponding to different elements or groups of elements into so-called "charge groups". The charge groups defined for the $D_1 - D_2$ range are: protons; (He-3, He-4); (Li, Be, B); (C, N, O); $Z \geq 10$ nuclei. In a similar way, charge group boundaries for particles stopping in D_3 are defined by equation (2) with suitable pairs of (a_i, b_i) values. A different functional form is required in this case because of the pronounced curvature of the ΔE vs. residual E tracks resulting from the large thickness of D_3 relative to D_2. The same charge groups as before are defined for the $D_1 - D_2 - D_3$ range, with the addition of a high-Z group corresponding to $Z \geq 20$. As an example of the implementation of this technique, the boundaries corresponding to the (C,N,O) charge group are illustrated schematically in Figure 10 for the $D_1 - D_2 - D_3$ range.

Each of the charge groups has an associated counting rate register which is incremented each time a valid event within the group is observed. In the spacecraft prime (real-time telemetry) mode, accumulation intervals are 32 s for the proton and alpha particle rate channels and 128 s for the heavy ion rate channels. In addition to providing counting rate information, the PI output is used to generate a 4-bit event code that controls the Event Priority System. The latter is included in order to maximize the LET PHA data-collection efficiency for the rarer nuclear species in the cosmic ray flux. Such a system is needed because the LET telemetry allocation (52 bits per s at the highest bitrate) limits the number of PHA events that can be transmitted to a maximum of 1 per second. Each pulse-height analyzed event is assigned a 4-bit priority value on the basis of its event code via predefined sequences stored in a ROM. Only the pulse heights corresponding to the highest-priority event occurring within every 1 s sampling period are transferred to the telemetry stream. The sequence of priority assignments for all event codes is changed periodically in order to prevent biasing effects. In addition to pulse height data and proton, alpha and heavy ion rates, the LET data frame contains digital status information and analogue housekeeping values, as well as counting rate data for the individual detectors. Housekeeping information includes instrument voltages, the detector leakage currents and temperature values for the detector telescope and electronics. A summary of the LET digital data channels is given in Table 4.

Also included in the instrument is an In-Flight Calibrator (IFC) circuit that checks, on command, the electrical characteristics of the instrument by delivering a sequence of pulses having well-defined amplitudes to all amplifier inputs.

4.1.1. *LET performance in-flight.*

The LET aperture cover was opened by means of the pyrotechnic actuators on October 19. On COSPIN turn-on four days later, all housekeeping data indicated that the instrument status was nominal, and the scientific data showed that a moderate solar flare event was in progress at the time of switch-on (see Fig.5). Further details of LET observations for this period are given in Section 3 of this paper.

Another example of LET data acquired in flight soon after turn-on is presented in Figure 11, in which we show pulse height information plotted in the ΔE vs. residual E format for protons and helium particles stopping in D_2. The data cover a 4-day period starting at 00:00 hrs UT on 7 November 1990, at which time a series of impulsive solar flare events occurred on the Sun. Such events are known to produce an enrichment in the isotope ^{3}He relative to the usually more abundant ^{4}He. Figure 11 shows that both isotopes were present throughout the period and were well resolved by the LET.

In addition to the initial flight data from the Ulysses instrument presented above, essentially identical LET sensors that were flown on the Phobos 1 and 2 space probes have provided a wealth of data on the solar and interplanetary energetic particle populations during the rising phase of solar cycle 22 [Marsden *et al.* 1990, 1991]. Fi-

nally, a substantial database on the performance of the LET has been accumulated during ground testing; the instrument has been extensively calibrated at particle accelerator facilities, with exposures to both heavy ion and proton beams [Kamermans *et al.* 1980; LeBorgne *et al.* 1981; Marsden *et al.* 1984].

The in-flight performance of the COSPIN LET instrument has matched that expected from ground calibration and test. While the majority of single detector counting rates are dominated by counts produced by the RTG neutron and gamma ray background, all coincidence channels show good immunity to RTG induced backgrounds. An exception is the low energy 0.3 – 1.5 MeV electron channel, which is dominated by the RTG contribution except during large solar particle events and, we expect, in Jupiter's magnetosphere. The performance in flight so far demonstrates that the experiment is capable of making important contributions to our knowledge of the particle populations in the heliosphere during the exploratory out-of-ecliptic Ulysses mission.

4.2. THE ANISOTROPY TELESCOPES (AT).

The ATs sensor unit consists of two, identical charged-particle telescopes, each with a geometrical factor of 0.75 cm^2sr, whose role is to measure the three-dimensional charged-particle distribution in the energy ranges 0.7 to 2.2 MeV for $Z \geq 1$, 2.2 to 6.5 MeV for protons, and 3.1 to 23.0 MeV for $Z \geq 2$. The three dimensional distribution measurements are achieved by inclining the two telescopes at independent angles (AT1 at 145° and AT2 at 60°) to the spin axis of the spacecraft and sectoring (8 sectors) the data outputs of the telescopes during each spin.

4.2.1. *Physical characteristics.*

The AT unit, which is situated at the top of the SIM-1 package shown in Figure 8, comprises two telescopes, each with independent electronics systems. Figure 12 shows a cross section of a single telescope. It consists of a stack of three semiconductor silicon surface-barrier detectors surrounded by a passive aluminium collimator shield which defines the 70° full-opening angle of the telescope. The front detector has a nominal thickness of 30 μm and a sensitive area of 2.0 cm^2, while detectors B and C are each of thickness 300 μm and have areas of 4.5 cm^2 each.

The exposed surface of the front detector has an evaporated layer of aluminium of 60 $\mu g/cm^2$ on it to reduce optical sensitivity, and has an 8 micron thick foil of aluminized kapton over it to eliminate optical effects and provide physical protection. It also eases the thermal balance problems of the telescope. All three detectors are operated at depletion voltage plus 50% to minimize radiation damage effects.

The C detector is operated in anti-coincidence with the A and B detectors and therefore provides active shielding over the reverse cone of the telescope. The forward acceptance cones of the telescopes are defined by the passive aluminium collimator shield which imposes a minimum low energy cut-off of 20 MeV for protons and 1.35 MeV for electrons. This reduces contamination of the energy channels to < 10% for an omni-directional E^{-2} differential spectrum, which is reasonable at these low energies. Should a differential spectrum of E^{-1} be observed at energies below ~ 100 MeV, a contamination correction may be necessary.

Inside the collimator are a series of matt black anodized baffles to reduce scattered sunlight and to scatter away energetic electrons which could be reflected onto the front detector. The electron and proton responses of the telescope are discussed below.

Figure 13 shows a functional block diagram of the electronics of a telescope. The outputs of the 3 detectors are combined to define a series of energy channels, which are shown in Table 5. There are two specific features of Figure 13 that need to be commented on. One is the In-Flight Test Generator (IFTG) and the other is the Reconfiguration Logic. The IFTG can be activated by command to produce a series of pulses which check the functioning and stability of the discriminator levels via the amplifier chain. It has an automatic switch-off mode as well as a commanded-off mode. The Reconfiguration Logic is designed to minimize the effects of possible electronic failures during the long time scale of the Ulysses mission, and permits some modification of the channel logics. Since the A1 discriminator plays a key role in enabling the logic, if it should fail its role is automatically assumed by the A2 discriminator, albeit at the trigger level of A2. As a part of the independent electronics chains, each telescope has an independent command-receive system.

The purpose of the digital data system is to organize the data suitably prior to it being read into the CPU. An outline of the system is given in Section 4.6, but in essence, during any one spin of spacecraft the data are routed into the appropriate one of the eight equiangular sector accumulators, and a data sample is composed of an integral number of spacecraft spins. Thus the data-collection time corresponds to this integral number of spin periods and is asynchronous with the (fixed) telemetry sampling rate. The data system deals with this problem by suitably adjusting the integral number of spins per sample period to remain "in-step" overall with the telemetry sampling period.

This system is used to give some of the energy channels both spin averaged and sectored outputs, as shown in Table 5. The sampling times shown are the average sampling periods, since the actual sampling periods corresponding to an integral number of spin periods. The sectoring for the $Z \geq 2$ (3.1 to 7.2 MeV) channel is reduced to quadrants to reflect the expected lower counting rates at these energies.

After processing by the data system, the data for each telescope is routed by its independent interface to one of the two processing units in the CPU for processing into the COSPIN data format. In contrast to other data channels in COSPIN, each AT is served exclusively by one of the redundant CPUs in the DPU.

4.2.2. *ATs calibrations.*

The electron response of the front detector of a telescope is minimized by the use of a thin detector and a high discriminator level (equivalent to 300 keV) for channel A1. The 30 micron detector corresponds to an effective range for an electron of 66 keV. The 300 keV discriminator can only be triggered by a 5-fold "pile-up" effect at this energy, or by electron "straggle" effects of electrons of 300 keV. Calculation indicates that a 30 micron detector has an efficiency of $< 10^{-3}$ for 300 keV electrons. This is compatible with electron accelerator tests using 200 to 400 keV electrons from the Van de Graaf accelerator at Harwell which indicate a detection efficiency of $\sim 2 \times 10^{-5}$ at these energies.

Additional electron accelerator tests have been done on the electron accelerator at the Herzberg Institute in Ottawa. These were performed at an energy of 65 keV to try to measure "pile-up" effects for electrons just coming to rest in the front detector. Interpretation of these results has proved complex, and a computer simulation of the electronics system is being used to produce a model that relates observed rates to actual rates. This is obviously an important tool for interpreting results during the Jupiter fly-by.

To calibrate channels A1 to A4 for particles with $Z \geq 1$, tests were done on the IBIS accelerator at AERE, Harwell, which gave protons up to 3 MeV. The minimum beam energy obtainable was 0.65 Mev. The "mid-point" energies of the measured thresholds have been used to define the energy ranges given in Table 5. The differences between calculated and measured values were small and above 2 MeV the measured edge agreed with calculated value.

Pre-launch calibration and test of the AT amplifiers was done using calibrated test generators, and the amplifiers are checked using the IFTG discussed above.

4.2.3. *In-flight performance.*

The instrument performance since switch-on has been good. The highest background counting rate, due to system noise, RTG induced counts and the cosmic ray background is in channel 1 (0.7 to 0.9 MeV, $Z \geq 1$), and corresponds to 0.05 particles cm^{-2} sr^{-1} s^{-1} for either AT1 or AT2. The background rates in the other channels are between a factor of 1.7 to 6 less than this. Overall the AT telescopes are providing satisfactory performance.

During the solar particle event starting on day 296, 1990 (cf Fig. 7), once particle isotropy had been established, the spin averaged counting rates observed by the two telescopes tracked each other closely. Similarly the spin averaged energy spectra and sectored counting rates also compared closely. This is also true of the other events observed.

Of more interest is the behavior during the initial stages of an event. Figure 14 shows the sectored counting rates at a time when the particle intensity was still rising. AT2 (looking sunward, in the direction of the spin axis) saw a markedly anisotropic distribution and a significantly higher intensity than telescope AT1 (viewing "backscattered" particles) which saw a lower intensity, largely isotropic distribution. For proton spectra derived from a fit to the integrated fluxes in the energy ranges of the AT channels, neither a power law nor an exponential in energy gives a good fit for this event.

4.3. THE HIGH ENERGY TELESCOPE (HET).

The high energy telescope (HET) is a large geometric factor cosmic ray telescope that uses particle trajectory determination together with the dE/dX vs. residual E technique to measure the energy and identify the mass and charge of cosmic rays. As shown in the photograph of the SIM2 unit in Figure 15, the HET with its analogue and digital electronics forms the largest part of SIM2, with the HFT, discussed below, mounted on top. A schematic cross-section of the telescope is shown in Figure 16. Detectors $D_1 - D_6$ provide signals that allow determination of the trajectory of the incident particle, and detectors $K_1 - K_6$ provide accurate measurement of the energy loss rates and total energy of particles which stop in the K detectors. For particles which stop in the detector stack, the telescope provides charge and mass resolution sufficient for studies of the chemical and isotopic composition of cosmic rays from hydrogen through nickel ($1 \leq Z \leq 28$). Approximate energy ranges for chemical and isotopic composition measurements as a function of Z are shown in Figure 2.

Through measurements of the intensity and chemical and isotopic composition of nucleonic cosmic rays with energies of order 10 through a few hundred MeV/nucleon, the telescope provides data relevant to a number of important questions in heliospheric and galactic cosmic ray physics, including acceleration of particles in solar flares, the nature of solar modulation, the structure of the heliospheric modulation region, the characteristics of the interstellar medium, conditions in the acceleration region itself, and results of nucleosynthesis in supernovae. In addition, the telescope provides measurements of electrons with energies of a few MeV for investigation of the propagation of solar and Jovian electrons throughout the heliosphere.

4.3.1. *Physical characteristics.*

Physical characteristics of the detectors and of the foils used as protective shields in the telescope are given in Table 6. Detectors $D_1 - D_6$ are multi-strip position sensitive Li-drifted silicon solid state detectors that measure both the energy loss in the detector and the location (by strip number) of the cosmic ray trajectory through the detector. The detectors were developed and fabricated at the University of Chicago (Lamport *et al.* 1976), and are operated at a bias voltage of 35 volts. As shown in Figure 17, the electrical contacts on the front surface of the detector consist of evaporated gold strips which are individually connected to a resistive divider chain on the detector ring, one end of which is connected to ground. On the back surface, a single evaporated aluminum contact covers the entire sensitive area of the detector. Thus, two signals are derived from each detector. The signal from the back surface (E signal) measures the total energy lost in the detector, while the signal from the front surface (P signal) is proportional to the location along the resistive divider chain of the strip in which the charge was collected. The position resolution achieved by this technique in the individual detectors is approximately 150 microns. With the strips of successive detectors (e.g., D_1, D_2, D_3) rotated by 60°, the trajectory of incident cosmic rays can be determined to an accuracy of better than 1°, as verified by accelerator calibration. Furthermore, use of three detectors in both the front ($D_1 - D_3$) and back ($D_4 - D_6$) planes provides a viable position-sensing backup in case one of the detectors fails during the mission.

Detectors $K_1 - K_6$ are thick (nominal 5 mm) Li-drift silicon detectors that, in combination, provide approximately 7 g cm^{-2} for stopping incident cosmic rays. Detectors $K_1 - K_4$ were supplied by the Lawrence Berkely Laboratory, and detectors K_5 and K_6 were supplied by the Kevex corporation. The $K_1 - K_6$ detectors are operated at a bias of 650 volts, which provides better than 99.5 % charge collection within the amplifier shaping time constant of ~ 5 microseconds. Anticoincidence protection for the telescope is provided by a scintillator shield (S) surrounding the telescope, and by a solid state detector, A, which identifies particles which completely penetrate the telescope.

4.3.2. *Functional description.*

A schematic block diagram of the electronics for the HET is shown in Figure 18. Signals from the front and back surfaces of $D_1 - D_6$ and from $K_1 - K_6$ (18 signals in all) are fed through charge-sensitive amplifiers and two sets of shaping post-amplifiers. Signals from $K_1 - K_6$ and the E signals from $D_1 - D_6$ are fed to a fast (1 microsecond shaping time constant) set of amplifiers to provide inputs for discriminators which, through the digital logic, are used to identify the particle type for counting rates and to set logic flags. In parallel, all 18 detector signals are fed to a slower (5 microsecond rise to maximum) dual-gain set of amplifiers which provide shaped signals for accurate amplitude measurement by the pulse height analysis circuitry. Gains for the dual-gain amplifiers are selected based on signal size as determined by discriminators operated off the differentiated rise of the charge-sensitive amplifier signal. To maintain the accuracy required for isotopic resolution through iron, the amplifiers in the PHA chain have been designed for extreme stability, and tests have demonstrated a drift in gain of $< 0.007\%/°C$ over the temperature range - 20°C to + 23°C. Gains and thresholds are monitored by an in-flight calibration sequence which is normally performed monthly, initiated by ground command.

If the combination of fired discriminators satisfies one of the logic conditions required for pulse-height analysis, output from the amplifiers goes to two peak-detector/sample-hold circuits that hold the signal amplitudes for processing by two 4096 channel (12 bit) analogue to digital converters, each of which processes 9 of the signals. Total processing time for a complete event is approximately 2 ms. The pulse height analysis data for an individual event consists of 280 bits containing the 18 pulse height analyses described above and 64 flag bits describing the state of discriminators attached to the individual detectors, the command state of the instrument, and the spin phase, divided into 8 sectors, at the time that the event was detected. Six HET PHA events are recorded during each spacecraft telemetry format period, or 32 seconds at the nominal bit rate.

Since the actual event rate in the telescope is much higher than can be returned as PHA data with the available telemetry, the PHA can only sample the events recorded by the telescope. To maximize the scientific return from the PHA sample, three priority levels have been established to govern selection of events for retention in the PHA sample. The actual logic for the priority levels (P) is given in Table 7 and the energy ranges as a function of the particle charge Z are shown in Figure 19. The levels correspond, roughly, to heavy nuclei which stop in the telescope (P_1), to any particle which stops in the telescope without triggering the anti-coincidence after penetrating at least to detector D_4 (P_2), and to any nucleonic particle which triggers detectors D_1 and D_2 but not detectors A and S (P_{3a}), or, with a 50% duty cycle, to any particle which triggers D_1, D_2, and D_4 (P_{3b}). P_{3b} includes both high energy penetrating particles and background events. P_3 is the lowest priority, and any P_3 event can be displaced by a P_2 or P_1 event. Similarly, any P_2 event can be displaced by a P_1 event. In quiet times since turn-on of the HET, about 40% of the events have been of type P_3, and of the order of 1% have been of type P_1.

In addition to pulse height analysis, the HET provides 29 digital counting rates. Of these 13 are derived by logic

from the discriminators to correspond to electrons, protons, and heavy nuclei in well defined energy ranges. The counting rates are true spin averages, with accumulation intervals of an integral number of spins, as determined by the software of the data processing unit, described in Section 4.6. Two counting rates provide 8 sectored anisotropy information for protons and electrons, while the remaining 14 counting rates monitor the counting rates of individual detectors as a housekeeping function. The characteristics of the counting rates are more fully described in Table 7. Energy ranges are based on computations from range energy tables for nucleons. All counting rates are telemetered to earth in 27 - -> 12 bit compressed format.

Because of the duration of the mission, the possibility of a detector failure must be considered, as noted above. Consequently a number of commands have been implemented to allow reconfiguration of the telescope logic to compensate for failure of one or more detectors. As shown in Table 8, the telescope logic is fully protected to the extent that every term in the logic can be modified in a predetermined way by ground command. In addition, there are commands to turn off high voltage supplies, to initiate (and turn off) the in-flight calibrate sequence, and to control power to three small heaters mounted in the analogue electronics of the HET to help maintain a stable thermal environment throughout the mission.

4.3.3. *Calibration.*

The HET unit now on the Ulysses spacecraft was tested on several occasions from 1982 - 1989 using beams of heavy nuclei from Ne through Fe accelerated by the Lawrence Berkeley Laboratory Bevalac. The calibration data have been used to verify proper function of the telescope, to characterize the detector response, and to develop algorithms for selection of the data and for determination of mass and charge of incident particles by use of the multiple dE/dx vs. residual E plus trajectory information returned by the telescope. An example of the calibration data, showing clear resolution of charges and isotopes in the immediate sub-iron region is shown in Figure 20.

Electron response was investigated over the energy range 3-35 MeV making use of a linear electron accelerator at the University of Chicago Argonne Cancer Hospital. Electron energy ranges were found to be very broad and poorly defined since no effort has been made to optimize the telescope for electron response. Some uncertainty remains in the calibration results also because of the difficulty of using the accelerator at the very low intensities required for our tests. The electron energy ranges given in Table 6 should therefore be considered preliminary. Further experimental work on the electron calibration using the flight spare HET is planned.

Response to the RTG radiations was tested using a simulated RTG (sRTG) at JPL in 1982 and, immediately before launch, by exposure to the flight RTG during the RTG mating test at the Kennedy Space Center (KSC). Initial tests with the sRTG showed RTG-induced events in prime HET data channels at intensity levels comparable to those expected from galactic cosmic rays. After adjustments of discriminator thresholds and modifications to the telescope logic the level of interference was shown to be markedly reduced by a second exposure to the sRTG. To further reduce background from the RTG's, a 1.6 kg tungsten shield was placed between the SIM-1 and SIM-2 units (Fig. 4). The configuration and placement of the shield was determined by use of Monte-Carlo techniques to provide the maximum shielding effect for the allotted tungsten mass given the known locations and shapes of the RTG radiation source and the detectors to be shielded. Since detectors $D_4 - D_6$ are key detectors for the HET pulse height analysis priority system and logic and for the electron counting rates $(H_6 - H_8)$, they were chosen as the detectors in which the maximum possible reduction in the rate of RTG-induced events should be achieved. Tests at KSC and in-flight experience show that the strategy was effective, and that RTG-induced events no longer make significant contributions to HET data channels except for the H_1 and H_6 counting rates, which, during quiet times, respond primarily to RTG-induced events.

In flight, an in-flight calibrator (IFC) is commanded on once per month. The IFC provides an exhaustive check of the gains and non-linearities of each amplifier by presenting at the inputs to the charge sensitive amplifiers a series of 2048 pulses, timed to the readout cycle, which cover the entire dynamic ranges of both the high and low gain amplifiers used in the pulse-height analysis. A normal IFC run consists of two passes through the pulse sequence, and requires approximately six hours at the nominal cruise telemetry bit rate. In addition, housekeeping channels monitor the regulated voltage lines that supply the amplifiers and the detector biases, the temperatures of the detectors and electronics, and the zero-offset of the digital to analogue converter (DAC) of the IFC.

4.3.4. *In-flight performance.*

Since turn-on day 296 (October 23) of 1990, the HET has functioned normally, and has been returning good data through all channels. Selected counting rates are shown in Figures 5 and 6 for the time from turn-on through the end of 1990. All other counting rates listed in Table 7 are also returning useful data, although, as expected from prelaunch tests, in the absence of a solar particle event the counting rates H1 and H6 respond primarily to the RTG-induced background at the levels indicated by the final RTG test at KSC.

The energy spectrum from the HET shown in Figure 7 for the solar particle event in progress on Day 296, 1990 (event a in Fig.5) shows that the derived absolute fluxes are consistent with fluxes measured by the other COSPIN telescopes. For the pulse-height analysis data, the tra-

jectory system is performing as expected, and Figure 21 shows the distribution of trajectories for particles heavier than protons as they pass through an $x - y$ plane midway between D_3 and D_4, as determined by the trajectory system. Figure 22 demonstrates the effectiveness of the trajectory correction in improving the charge and mass resolution of the telescope in response to an isotropic flux by comparing the appearance of sample dE/dX vs. E cross plots before (Fig. 22a) and after (Fig. 22b) application of a preliminary correction for the trajectory as determined in $D_1 - D_6$. The data in Figure 22 include all heavy nuclei stopping in the detectors $K_2 - K_6$ during 118 days of data, including particles entering over the full range of acceptance angles of the telescope. The analysis is still preliminary, and further improvements can be expected as the number of events collected increases, and as our understanding of the system develops. At the current, near-solar-maximum phase of the solar modulation cycle, Fe nuclei are being collected at the rate of approximately one per day during quiet times.

4.4. The high-flux telescope (HFT).

The HFT is designed: (a) to provide measurements of protons, helium, and heavier particles when the fluxes are too intense for the larger telescopes, and (b) to provide an instrument with exceptional azimuthal resolution so that highly collimated field-aligned particle distributions can be measured if they are encountered, especially over the solar poles and in Jupiter's magnetosphere.

4.4.1. *Physical characteristics.*

The HFT, which is mounted on top of the HET (cf Fig. 15), consists of a single 25 mm^2 × 18 μm silicon surface-barrier detector, passively collimated by a fan-shaped aluminium collimator to give a viewing aperture of 17° × 60°, with a geometrical factor of 0.033 $cm^2 - sr$. The telescope cross sections are shown in Figure 23. The collimator imposes a low-energy cut-off of 50 MeV for protons and 5 MeV for electrons incident from outside the viewing aperture. The exposed surface of the detector carries an evaporated layer of aluminium 0.25 mg/cm^2 thick to exclude light and attenuate low-energy protons, which would cause serious pulse pile-up when the flux is large and the energy spectrum steep, as in the inner Jovian magnetosphere. The absorber excludes protons below 80 KeV and electrons below 10 KeV. There is a small sensitivity to directly incident sun light which slightly increases the detector leakage current when the instrument is viewing the Sun. The thinness of the detector, the high discriminator levels, and the fast shaping time constants used in the electronics make the HFT very insensitive to electrons. The detector output is amplified and shaped using double-differentiation time constants of 100 ns to provide bipolar pulses that can be handled without excessive loss or base-line shift at rates up to 10^6 per second.

Five discriminator channels (designated $F_1 - F_5$) set at levels corresponding to energy depositions between 0.20 and 36.0 MeV define the energy ranges given in Table 9. The F_1 discriminator can be set by command to any one of 16 threshold levels between 0.20 and 4.3 MeV. Alternatively, F_1 can be commanded into a stepping mode where the discriminator cycles continuously through the 16 levels at a rate of one step per data accumulation period (16 seconds at a telemetry data rate of 1024 bits/s). The stepped mode has been selected for normal mission operations. The F_2 discriminator can be set by command to two levels corresponding to 0.21 and 0.50 MeV, respectively. Channels F_3, F_4, and F_5 are set at levels 2.45, 8.36, and 36.0 MeV, respectively. F_1 levels 0-2 and F_2 levels 0-1 respond primarily to protons. F_1 levels 3-13 and F_3 respond primarily to helium. F_4 responds primarily to the CNO group. F_5 responds primarily to S and the Fe group. The F_2 output to the DPU can be scaled down by a factor four on command when it is expected that the rate may exceed the capability of the DPU interface unit, as during Jupiter encounter.

The instrument includes an internal, dual range, 128-step pulse generator for in-flight calibration of the discriminator triggering levels.

The instrument is mounted so that the collimator "fan" plane lies parallel to the spacecraft spin axis. The central axis of the detector and the collimator is set at an angle of 45° with respect to the Earth-pointing end of the spin axis so that the aperture extends from a spacecraft polar angle of 15° to 75°. All HFT counting rate accumulation intervals are spin synchronized using the Ulysses spacecraft sun reference pulse. Channels $F_1 - F_5$ are each accumulated for an integral number of spins every telemetry read out. The output of channel F_2 is also sector accumulated using 32 sectors per spacecraft rotation (11.25° per sector), which permits the recognition of highly collimated angular distributions with a resolution of $\approx$ 20°. To conserve storage and telemetry facilities, eight equispaced sectors are successively accumulated for an integral number of spacecraft rotations having a nominal average period of 32 spacecraft minor frames. During the period over the solar poles and during an adjacent 18-month period, the angle between the assumed direction of the interplanetary magnetic field and the spin axis will lie in the range 40° ± 25°, so that the field direction will be included within the HFT aperture at some time during each spacecraft spin period.

4.4.2. *HFT performance in high particle fluxes.*

At closest approach to Jupiter ($\approx 6\ R_j$), from Pioneer 10/11 and Voyager 1/2 reports we estimate the electron intensity > 10 KeV to be $\approx 10^8\ cm^{-2}s^{-1}sr^{-1}$, or $3 \times 10^6 s^{-1}$ within the acceptance angle of the telescope.

This is on average ≈ 0.3 particles per 100 ns, with an average deposit of 15-20 KeV per particle (the maximum energy deposit is $\approx$ 60 KeV). The high order of pile-up required to trigger the 200 KeV discriminator makes electron contamination of this channel unlikely. Electron pile-up studies have been performed at NRC using a small electron accelerator facility.

At $L \approx 7$ R_j where the proton flux reaches a maximum, we estimate that for energies greater than a specified energy, E, and a $dJ/dE \propto E^{-3}$ spectrum, the integral proton flux through the detector will be $\approx 2 \times 10^5$ $E^{-2}\text{cm}^{-2}\text{s}^{-1}\text{sr}^{-1}$ at energies around 1 MeV. If this energy dependence persists down to low energy (50-100 KeV), the proton pile-up would, in the absence of an absorber in front of the detector, saturate the 0.20 MeV discriminator, and this effect would be appreciable out to $L = 10 - 12$ (where L is the McIlwain parameter which is equivalent to R_j at the equator). The presence of the 0.25 mg/cm^2 Al absorber significantly extends the intensity range where proton pile-up is unimportant.

Since the alpha particle discriminator F_3 is set at 2.2 times the maximum energy deposition by protons, it requires a three-fold proton pile-up to simulate an alpha. At $L = 7$, the proton contamination of the F_3 alpha channel is estimated at less than 10% and for $L > 9$ it is negligible. In interplanetary space, the highest counting rates expected at the lowest discriminator levels are in the $10^3 - 10^4$ s^{-1} range, well below the level where pile-up or loss is significant.

4.4.3. *HFT performance in flight.*

The post-launch performance of the HFT has been nominal in all respects. Except for calibration periods, the HFT has been operated with the F_1 discriminator in stepped mode and the F_2 discriminator set low. Periodic spikes in the HFT detector current monitor channel were observed following instrument switch-on with a period of 4064 ± 16 seconds. This effect is caused by sunlight incident on the detector. The period is a function of the HFT view cone, the spacecraft spin period and the 32 second sampling of the detector current. Some sensitivity to sunlight had been expected from bench tests prior to instrument delivery and it was a relief to find that the maximum observed amplitude ($\sim$ 80 nA) was well below the level which would cause any increase in system noise.

It is possible to extend the proton and helium energy spectra derived from the other COSPIN sensors down to about 0.3 MeV/nucleon using the F_1 stepped discriminator channel. Using an assumed spectral form for the proton and helium differential energy spectra, the free parameters are determined by a best fit to the 16 F_1 counting rates. This analysis has been performed for the period $\sim$ 1700 to 2400 UT on day 296 just after instrument switch-on and yields reasonably consistent flux values with the LET, HET, and KET (cf. Fig. 7).

Figure 24 shows a period with an unusually large anisotropy in the F_2 sectored rate. While positional and magnetic field data are not yet available for the period, the direction of the anisotropy is consistent with outward streaming from the Sun along the nominal magnetic field direction. The HFT view cone lies at 45° to the Ulysses $+Z$ axis in the $+XZ$ plane. This is the standard reference plane for the generation of the Ulysses Spin Reference Pulse and the start of F_2 sector 0. During the period shown, Ulysses was approximately one week past first opposition and was slightly lagging the Earth in its trajectory around the Sun. The HFT because of its 45° orientation to the $+Z$ axis should be looking almost directly antiparallel to the sunward direction along the nominal interplanetary magnetic field when the $+XZ$ plane is 180° past the Sun crossing.

4.5. THE ELECTRON TELESCOPE (KET).

As shown in the photograph in Figure 25 (see also Fig. 4), the KET consists of two separate boxes, SIM3A and SIM3B, mounted on the other side of the spacecraft platform with respect to the SIM1 and SIM2 units. SIM3B is the telescope portion of the KET, and SIM3A contains the analogue and digital electronics for the KET.

The KET is designed to measure electron fluxes between 2.5 and 6000 MeV, and to determine energy spectra in the range 7 – 170 MeV. The telescope also provides measurements of the proton and alpha-particle fluxes in several energy windows between 3 and $>$ 2100 MeV/nucleon. In addition, two low-energy electron and proton channels provide anisotropy information in 8 sectors. (see Table 10).

The determination of electron spectra and their variation with distance from the sun and solar latitude provides vital information on the solar modulation of interstellar electrons as well as on acceleration and propagation of interplanetary and solar electrons. The measurement of protons and helium nuclei with the same telescope enhances confidence in the calibration and response of the telescope, and permits investigation of the dependence on particle species of the effects of solar distance and latitude.

4.5.1. *Physical characteristics.*

To reduce mass and complexity of the instrument, the KET consists of two separate parts: the sensor (SIM3B) and the electronics box (SIM3A), both mounted beneath the spacecraft platform, as shown in Figure 4. A cross-section of the telescope is shown in Figure 26. The telescope is mounted to view perpendicular to the spin axis and has an acceptance angle of 44.6 degrees full cone with an auxiliary field of view of 106 degrees. Accordingly, for nuclei the geometric factor varies between 0.72 cm^2 sr for particles reaching D_2 and 6.5 cm^2 sr for particles stopping in D_1. A more sophisticated evaluation of the geometric

factor taking into account energy dependence and effects of scattering and shower production for electrons is shown in Table 10. The instrument incorporates several techniques in order to identify the particles and their energies: electron-photon cascades, Cherenkov thresholds, dE/dx *versus* E method, and discriminator settings. Functionally, the detector system divides naturally into two parts, consisting of an entrance telescope and a calorimeter surrounded by a guard counter.

The entrance telescope is composed of a silica aerogel Cherenkov detector C_1 inserted between two surface-barrier semiconductor detectors D_1 and D_2. Together with the guard counter A, it defines the geometry and selects singly-charged particles of high velocity ($\beta > 0.938$) to discriminate between electrons and protons. In conventional designs the velocity discrimination is performed using a high-pressure-gas Cherenkov detector. The availability of a low-density solid material like silica aerogel, which can have a refractive index as low as 1.02 to 1.2, which is translucent and which shows a negligible scintillation contribution to the signal, allows us to circumvent the disadvantages of a gas Cherenkov detector, which include a significant weight penalty and additional material in the acceptance cone. For use in the KET, we have chosen an aerogel with a refractive index of $n = 1.066$. Since no use is made of the directionality of the Cherenkov light, the block of aerogel is placed in a diffusion box with millipore walls. The light signal of C_1 is viewed by the phototube PM1 through a hole in the guard counter, A. To prevent particles from hitting the photocathode of PM1 directly, and thus simulating an aerogel detector response, a scintillator disc S_1 has been introduced in front of PM1 as a veto counter. S_1 gives a signal for minimum ionizing particles 6 sigma above the signature of relativistic alpha particles in aerogel.

The calorimeter consists of a lead-fluoride crystal C_2 in which the electron shower develops, and a scintillator cup S_2 to detect particles not absorbed in C_2. C_2 has a thickness of 2.2 cm, corresponding to 2.5 radiation lengths.

Lead-fluoride was chosen for its short radiation length $\left(X_0 = 6.6\ \mathrm{g/cm^2}\right)$, its high density $\left(\rho = 7.7\ \mathrm{g/cm^3}\right)$, and its convenient refractive index ($n = 1.885$). Furthermore, it does not scintillate and is thus relatively insensitive to the RTG background. The Cherenkov light of C_2 is viewed through a hole in S_2 using a diffusion-box design. To prevent particles from escaping undetected through the hole in S_2, the planar part of the cup has been extended.

The scintillator A not only helps to define the sensor geometry, but also protects from background caused by nuclear interactions produced in the telescope by cosmic rays and by neutrons from the RTG. If experience in flight shows that shower development in the calorimeter reduces the effective geometry factor to an unacceptably low value, the discriminator threshold of A can be raised by telecommand for penetrating electrons only (channel E300).

To compensate for a possible phototube gain loss during the long mission lifetime, the high voltages can be stepped up by telecommand in eight steps. In the case of complete failure of a detector, it can logically be switched off by telecommand using the onboard failure reconfiguration logic. Stimulation of the onboard electronics for checkout purposes is also provided.

The data produced by KET consist of pulse height analysis data and coincidence counting rates corresponding to broad energy ranges for incident particles. The ranges and time resolutions for the counting rates are shown in Table 10. Pulse height analysis is performed on a sample of the incident particle events to provide good energy resolution (between 60 and 100 % for electrons) and clear identification of particle species. Single-detector counting rates and housekeeping data are also telemetered to monitor instrument performance.

4.5.2. *Instrument calibration.*

The KET instrument measures cosmic ray electrons with energies from a few MeV to several GeV, which have a flux in the ecliptic plane 3 to 4 orders of magnitude lower than the proton flux. The instrument response was therefore extensively calibrated with both electrons and protons. The most important goals of these calibrations were:

- to determine the response of the individual detectors as a function of particle species and energy
- to determine the detection thresholds for the individual detectors, especially the Cherenkov thresholds of C_1 and C_2
- to determine the energy thresholds for the coincidence counting rate channels
- to provide correction tables for the counting rate data (response matrix)
- to determine the electron detection efficiency of individual counting rate channels and of the complete instrument as a function of energy
- to determine the proton rejection rate for electron channels
- to use the calibration data to verify and adjust the mathematical model of the instrument
- to determine the background in the various counting rate channels due to the RTG

Results of proton calibrations

The main goals of the proton calibrations were to determine proper settings for i) the Cherenkov thresholds of C_1 and C_2, and ii) the discriminator threshold values C_{10}, C_{20}, and S_{20}, this last one being actually determined by the range of the particles in the telescope. In addition, these calibrations provided measurements of key parameters such as angular response and sensitivity of the anticoincidence which define the effective geometry factor of the instrument.

Results of electron calibrations

These calibrations resulted in the measurements of: i) the response of the calorimeter C_2 as a function of energy, the monoenergetic response of C_2 being of fundamental importance to determine the electron spectrum from the flight data, and ii) the variation of the efficiency and response of the telescope as a function of energy and incidence angle.

It was possible to determine relative variations of the response of the detector with energy and incidence angle of the beam. However, it proved to be extremely difficult to measure the absolute efficiency for electrons, particularly at low energies, where the use of external counters to monitor the beam is impossible because of the large scattering they induce. Therefore, only the relative efficiency could be reliably measured.

The key results of these calibrations are shown in Figures 27 to 29. These figures display as a function of energy: the average C_2 signal (Fig. 27), the probability of absorption of the particles in C_2 (Fig. 28), and the relative efficiency of channels E_4, E_{12}, E_{300} (Fig. 29). For comparison with calibration data, some of these figures contain also the results of a Monte-Carlo simulation described in the following section.

Results of the RTG calibration tests

The RTG calibration of the KET was performed in 1985 at Mound Laboratories using the Galileo Flight RTG (F_3) and in 1986 and 1990 at KSC during the RTG compatibility tests as part of the two launch campaigns. The main results can be summarized as follows:

- RTG induced background in the instrument leads to a deadtime increase from 0.003 % to 0.5 %, which is a tolerable value. The main contribution to the dead time stems from the scintillation guard counter with its large field of view.
- From a scientific point of view, only the channels P_1 and E_4 are adversely affected, as the RTG background is of the order of the cosmic ray quiet flux in these KET particle channels, e.g. 1×10^{-3} counts/s in E_4. They will only produce meaningful data during solar flares and near Jupiter. Use of Cherenkov detectors and multifold coincidences guarantees the low susceptibility of all the other KET scientific channels.
- Between the RTG tests in 1986 and 1990 the KET observed an increase of the RTG background by about a factor of 2. This is attributed to time variations in the plutonium decay chain.
- Flight data measured during quiet times confirm the same background level in the RTG-sensitive channels P_1 and E_4 as observed during the 1990 RTG-test on ground.

Simulation of the telescope

In order to determine the absolute efficiency of KET for electrons, it was necessary to use a Monte-Carlo simulation of the instrument. The GEANT program, developed and widely used by particle physicists, was adapted for this purpose.

In a first step, the different parameters of the telescope, namely thresholds and detector resolutions, were adjusted in order to reproduce the calibration data obtained at the different accelerators, with a parallel beam in the axis of the instrument. An excellent agreement between the simulation and calibration results was achieved, as can be seen in Figures 27 to 29. This agreement ensures that we can reliably determine the efficient geometry factor of KET for an isotropic flux, which was done according to the method given by Sullivan (1971). This efficient geometry factor is shown in Figure 30 as a function of energy.

In-flight calibration

On COSPIN switch-on the currents and high voltage values were checked and found to be nominal. The in-flight test generator was used to check the amplifier gains and the functioning of the coincidence logic and of the failure mode reconfiguration. All of these were found to be nominal.

To measure the performance of the detectors, the linearity of the analogue chains, and the discriminator thresholds, it is necessary to use the cosmic ray data themselves. Protons and helium nuclei with an energy above 2.1 GeV/n can be used for this purpose since they are minimum ionizing particles that penetrate the telescope while producing almost no nuclear interactions in the detectors, and are above the Cherenkov threshold C_{10}. Their large flux allows collection in a few days of a sample with sufficient statistical accuracy to monitor all the detector responses and amplifier gains except for C_1 (for which no PHA value is registered). For P_{4000}, the in-flight responses are identical within a few percent to the responses derived from calibrations with a beam of 5 GeV/c protons. The position and width of the helium response for these detectors are also compatible with the expected values derived from the proton response.

The C_1 PHA are registered only in the E_4 and E_{12} channels, and therefore can be monitored only in these channels. The C_1 response for E_{12} particles is compatible with the calibration results for electrons of 7.5 and 10 MeV.

4.5.3. *Preliminary results.*

The results presented in this and in the previous section are obtained from the quick-look data only, transferred from JPL to our home institutes in Europe through the SPAN network. Although not complete, and with a quality lower than specified mission standard, these first data allowed us to extensively check the functioning of the KET. Moreover, they also allowed us to obtain the first, still preliminary, scientific data.

Figures 5 and 6 include hourly averages of the counting rates P_{116}, P_{190}, E_4, E_{12}, and E_{300} (see Table 10 for particle types and energy ranges). Several solar flares can be seen with varying electron to proton ratios. The October 23 solar particle event (event a in Fig. 5) is rich enough in electrons, protons, and alpha particles to derive a flare spectrum for each of these species.

The detailed study of low energy electrons in quiet time periods reveals that their flux shows variations related to favorable magnetic connections to Jupiter, as has been observed on other missions in the past (e.g., Chenette *et al.* 1977). From the switch-on date to the end of November Ulysses was presumably well connected to Jupiter, if one assumes an average value of the solar wind velocity, a parameter not yet available to us from flight observations. The average E_4 counting rate for this period is about 4.5×10^{-3}c/s with a quiet time increase to 5.5×10^{-3}c/s. It then decreases down to 3.5×10^{-3}c/s in December, as the connection to Jupiter becomes less favorable. During the same epoch the fluxes of high energy protons and helium nuclei increase by 15% (see Fig. 31) in accordance with the decrease of solar modulation. It is worth noting that these values are in excellent agreement with the low energy electron spectrum found by Moses (1987) with data spanning a 6 months interval in a period of good connection to Jupiter.

4.6. THE DIGITAL PROCESSING UNIT (DPU).

For the COSPIN experiment, the DPU is the mediator between the spacecraft and the experiment sensor subsystems. It collects scientific data and status information from the COSPIN telescopes and processes and formats them for transfer to the telemetry system of the spacecraft. It also receives and acts on commands from the spacecraft telecommand system to control the status of the COSPIN experiment as a whole, or of individual subsystems within COSPIN. The DPU is mechanically integrated into the SIM-1 package of COSPIN, together with the LET and AT sensors, as shown in Figure 4.

The DPU can be broken down functionally into the Central Processing Units (CPUs) and the User Interface Units (UIUs). Every sensor subsystem has a dedicated UIU, except for the HET and HFT, which share one unit.

The UIUs are jointly serviced by two CPUs, as indicated in the DPU block diagram (Fig. 32). The CPUs are identical in terms of hardware, and are based on the RCA 1802 microprocessor. The parallel structure of the CPUs extends into the spacecraft interface domain, and there is no direct communication between the CPUs. Of each telemetry frame, twenty 8-bit words are allocated to the COSPIN experiment, and ten words are supplied by each CPU. In the case of a severe malfunction in one unit, the offending side can be switched off by ground command, and the remaining CPU will supply the same data with half the time resolution. An exception is data channels for the ATs, since each of the two ATs is served exclusively by one CPU.

A CPU consists of the microprocessor, the program storage (ROM), the data storage (RAM), and the spacecraft- and UIU interface section. Since no connection exists between CPUs, they rely on spacecraft timing pulses (frame, format, Sun pulse) to synchronize their efforts. A CPU process cycle is complete in eight spacecraft formats (256 frames), and begins with the occurrence of the eight-format pulse. For counting rate accumulations, the 256 frames are internally divided into 2, 4, 8, and 16 time segments. Thus, the finest time resolution available for intensity measurements from COSPIN corresponds to the time associated with 16 frames of telemetry data (16 seconds at a telemetry rate of 1024 bits/sec). Pulse height analysis data from the LET, HET, and KET are handled differently. In each 32 frame spacecraft format, 32 PHA events are returned from the LET, 6 PHA events are returned from the HET, and 5 PHA events are returned from the KET. Average accumulation times for each event at a telemetry rate of 1024 bits/sec are 1 second, 5.33 seconds, and 6.4 seconds, respectively.

With the exception of the AT data channels, the software has been designed so that adjacent time segments for each data channel are processed by alternate CPUs. Data read from the UIUs are arranged into a format image in the RAM. The telemetry system requests ten 8-bit words per frame, which are sent through the direct memory access facility of the CPU. The read-in and read-out process is tied to the telemetry timing. By providing an adequate lag between both, the required telemetry information will be available in time and the CPU processing will also be independent of the telemetry rate.

A UIU can best be described as a collection of counting registers which receive event pulses from the experiment sensor subsystems. Each counter, or rate channel, accumulates events for a period of time and is then read out by the CPU. The accumulation interval may be related to the format time or the spacecraft spin as explained below. In addition, pulse-height analysis data are temporarily stored in the UIU until read out by the CPU. Complementary services such as storing the last command and buffering of timing and control lines are also provided by the UIU.

For each COSPIN sensor subsystem a single 8-bit bus connects both CPUs to the UIU. The CPU programs are arranged such that only one CPU places a request on the bus at any given time. The UIU monitors both CPU interfaces, and will respond when addressed. If the response requires the transmission of data, this will be done serially through a special return data line. Many circuits, in particular the more important rate channels and PHA buffers, are duplicated for improved reliability. Both CPUs have an independent connection to the telecommand system

of the spacecraft. The 16-bit command is composed of a 4-bit user address and a 12-bit user command. The CPU sends the command bits to the addressed experiment at a maximum rate of one command per frame.

Format-synchronous counting rate channels are used only by the LET. The accumulation period is 32 frames (one format), or 128 frames (four formats). All other counting rate channels are spin-synchronized. As the spin period is not related to the format timing, a mechanism must exist to achieve a pseudo-synchronism. This is achieved in the following way. Every class of spin-synchronous channels has a fixed nominal accumulation window of 16, 32, 64, or 128 frames associated with it. The start of a given spin-synchronized accumulation period coincides with the sun pulse from the spacecraft, which marks the passage of the $+X$ axis acrosss the center of the Sun. The end coincides with the completion of the spin during which the appropriate nominal accumulation window closes. The number of spins completed during each accumulation is counted in four spin counters corresponding to the four different nominal accumulation intervals. Sectored channels are treated essentially like spin-synchronous channels, but the input to the event counter is only enabled during one sector of each spin. Different sectoring signals exist to allow definition of sectored counting rates with 4, 8, or 32 sectors per spin.

The COSPIN experiment data are arranged in a 256 frame format. For reference purposes, synchronization words are inserted every 16 frames. Rate channel date are presented in a floating-point notation with word length of 8 or 12 bits, representing accumulation buffer sizes of 19 or 27 bits respectively. PHA data are stored as received from the sensor subsystem. There are also a number of DPU status words which carry additional operating information or signal conditions.

The DPU software includes a special backup memory mode of operation for use to partially fill in gaps between real time telemetry acquisitions if both spacecraft tape recorders should fail, or if it should happen that an anticipated gap between real time telemetry passes should exceed the maximum period for which data can be stored on the tape recorders. In this mode, which is entered by command, a limited number of readings of selected spin-averaged counting rate channels are taken at regular intervals and stored in the random access memory of the DPU until they can be read out during a real time telemetry pass. Normal operation is resumed by command. Up to 159 data samples may be collected, and depending upon the length of the anticipated gap, the interval between samples of the data channels may be chosen to provide coverage for periods from 5.6 to 45.2 hours (at 1024 bps). At lower bit rates, the maximum intervals of coverage are proportionately longer. The counting rate channels included are L_{4-11}, A_3, H_2, F_1, and K_{13-20}, defined in the Tables 4, 5, 7, 9, and 10, respectively. These counting rates provide information concerning time variations in fluxes of low energy protons (0.3 – 3.8 MeV) and electrons (4 – 12 MeV).

4.7. THE DC/DC POWER CONVERTER.

Two fully redundant DC-DC power converters located in box SIM-4 derive a set of secondary voltage rails from spacecraft + 28 V power system. An unregulated 8.5 V rail is used primarily to power digital circuitry in the experiment. A loosely regulated + 80 V rail is used mainly to power other high-voltage converters for PM tube and detector bias, and a + 35 volt rail is used directly for bias of detectors. Regulated rails at voltages of ± 15V, ± 10V and – 6V are used mainly for powering analogue circuitry.

The converters operate by first chopping the 28V primary and then successively transforming, rectifying, and regulating each output as necessary. Operation is synchronized to the 114.688 kHz spacecraft sync. clock using a phase-locked loop, while input and output filter circuits minimize conducted interference to systems. The efficiency of the units is better than 66%.

Acknowledgements.

The Principal Investigator (J.A.S.) appreciates the remarkable cooperative spirit and support of the COSPIN Consortium throughout the many years of our joint effort, and especially thanks K.-P. Wenzel, H. Kunow and R.B. McKibben for assuming special responsibilities in the Consortium.

We wish to acknowledge with gratitude the individuals in each group who contributed in many ways to the success of the COSPIN instrumentation or to the development of the software. Without their dedicated efforts and ingenuity our participation in the Ulysses mission would not have been possible.

For the Low Energy Telescope and the Data Processing Unit (ESA/SSD) – The authors wish to express their thanks to all those who have contributed to the success of the experiment. In particular, from ESA/SSD, T.F. Iversen, M. Trisch-Berger, L. Smit, R. Scheper, J. Fleur, S.T. Ho and M. Szumlas. Invaluable assistance during accelerator calibrations was provided by H. Crawford (LBL, Berkeley), H. Blok (V.U., Amsterdam), A. Mueller (GANIL, Caen) and E. Jaeschke (MPK, Heidelberg).

For the Anisotropy Telescopes and Data Processing Unit (Imperial College, London): We thank R. Burrows for the use of the electron accelerator at HIA; and R. Burrows, E.E. Budzinski and T. Cameron for their invaluable help during the calibration. Also Dr. T. Conlan and his colleagues at AERE, Harwell, for their assistance with the proton cal-

ibrations. The Imperial College experiment was supported by the Science and Engineering Research Council, UK.

For the High Energy Telescope (Laboratory for Astrophysics and Space Research, The Enrico Fermi Institute, University of Chicago): We are grateful to J.E. Lamport, M. Weber, H. Thomas, R. Gabriel, G. Ho, P. Kruley, G. Popelka, F. Sopron, J. Stepney, and H. Tibbs for their many and varied contributions to the design, fabrication, and test of the High Energy telescope experiment package, support equipment, and software required for analysis of test and flight data. The heavy ion beams provided by the Bevalac Accelerator (Lawrence Berkely Laboratory, University of California) for calibration and resolution tests of the HET have been essential for this mission and we wish to thank H. Crawford and F. Lothrop for their assistance. The University of Chicago program is supported by NASA/JPL Contract JPL 955432 and NASA Grants NGL 14-001-006 and NAGW-1981.

The High Flux Telescope (HIA/NRC, Canada): The mechanical design of the HFT was implemented by E.E. Boyce and J.D. Johnson. D. Graham was responsible for fabrication of mechanical parts for both the HFT and the HET. J.D. Johnson was responsible for parts procurement and quality assurance. Electrical and mechanical assembly was performed by E. Taada. L. Bradley and V. Sullivan designed and constructed the COSPIN Ground Support Equipment. (GSE) T. Berrens developed the ARAMIS language used for much of the COSPIN GSE software system. G. Mackey managed the contract with Spar Aerospace Limited for the design, construction and testing of the SIM-4 DC/DC power converter. I.B. McDiarmid was instrumental in ensuring the above effort was funded. Special thanks are due to all the above individuals and to the other unnamed NRC staff who contributed to the success of this mission. We also wish to thank the McMaster University tandem Van de Graaf facility for their support in the calibration of the HFT.

For the Kiel Electron Telescope (Univ. Kiel, Germany; CENS, France): The expertise of J.J. Engelmann greatly improved the KET sensor design. K.H. Stellmaschek contributed to designing, testing, and integrating the KET analogue electronics. Calibration and testing over long periods of storage and reintegration was supported by D. Mueller. The KET digital electronics was designed, implemented, and tested with the help of B. Jacquemin, A. Roy, J. Cretolle, and J.C. Courtois. E. Rode was responsible for design and fabrication of the KET mechanics which greatly benefited from design ideas of G. Salzmann. H. Glüer and H. Boll contributed significantly to the development of the KET data evaluation programs. For assistance with accelerator calibrations we thank the accelerator groups of Saclay, CERN, Orme de Merisiers, University of Bonn, and DESY. The KET experiment is supported by the Bundesministerium für Forschung und Technologie, the Centre National d'Etudes Spatiales, and the Commisariat a l'Energie Atomique.

We are grateful for the continual assistance given to the COSPIN Consortium by the Project Managers D. Eaton (for ESA) and W. Meeks (for JPL/NASA) and their teams, especially P. Caseley, W. Frank, H. Schaap, and G. Tomaschek for ESA, and M. Agabra, J. Haas, and T. Tomey for JPL/NASA. We are also grateful to the Dornier team, and especially to D. Kolbe, for their assistance during spacecraft integration and test.

References

Chenette D.L., Conlon T.F., Pyle K.R. and Simpson J.A. 1977 ApJ 215, L95

Kamermans R., Henrion J., Marsden R.G., Sanderson T.R. and Wenzel K.-P. 1980, Nucl. Instr. and Meth. 171, 87

Lamport J.E., Mason G.M., Perkins M.A. and Tuzzolino A.J. 1976 Nucl. Instr. and Meth. 134, 71

LeBorgne J.F., Henrion J., Marsden R.G., Sanderson T.R. and Wenzel K.-P. 1981, Report ESA STM-224

Marsden R.G., Henrion J., Sanderson T.R., Wenzel K.-P., de Bray N. and Blok H.P. 1984, Nucl. Instr. and Meth. 221, 619

Marsden R.G., Afonin V.V., Balazs A., Erdos G., Henrion J.P.G., Richter A.K., Rusznyak P., Somogyi A., Szalai S., Varga A., Varhalmi L., Wenzel K.-P. and Witte M. 1990, Nucl. Instr. and Meth. 290, 211

Marsden R.G., Afonin V.V., Witte M., Erdos G., Gringauz K., Richter A.K., Somogyi A., Varga A., Varhalmi L. and Wenzel K.-P. 1991, Planet. Space Sci., 39, 57

Moses D. 1987, ApJ 313, 471

Simpson J.A., Anglin J.D., Balogh A., Bercovitch M., Bouman J.M., Budzinsky E.E., Burrows J.R., Carvell R., Firth J., Garcia-Munoz M., Henrion J., Hynds R.J., Iwers B., Jacquet R.M., Julliot C., Kunow H., Lamport J.E., Lentz G.A., Marsden R.G., McKibben R.B., Müller-Mellin R., Perkins M.A., Raviart A., Rode E., Sanderson T.R., Scheper R.J., Stellmaschek K.H., Treguer L., Trischberger M., Tuzzolino A.J. and Wenzel K.-P. 1983, ESA Special Publication SP-1050, p.155

Sullivan J.D. 1971, Nucl. Inst. and Meth. 95, 5

Wenzel K.-P., Marsden R.G., Page D.E. and Smith E.J. 1992, A&AS (this volume)

TABLE 1. *Cosmic ray and solar particle investigations (COSPIN) instrumentation and participating institutions.*

INSTITUTION	INSTRUMENTATION
Laboratory for Astrophysics and Space Research, University of Chicago	High-Energy Telescope (HET)
Herzberg Institute of Astrophysics	High-Flux Telescope (HFT) Low-Voltage Power Converter (SIM-4) Experiment Checkout Equipment (EXPCOE-1A)
Blackett Laboratory Imperial College	Anisotropy Telescopes (ATs) User Interface Units (UIUs)*
Space Science Department of ESA, ESTEC	Low-Energy Telescope (LET) Central Processing Unit (CPU)*
University of Kiel	Electron Telescope (KET)
Centre d'Etudes Nucléaires de Saclay	KET Digital Electronics Checkout Equipment for KET (EXPCOE-1B)

* The UIUs and CPU together constitute the Digital Processing Unit (DPU)

TABLE 2. *COSPIN mechanical, data, and electrical-interface parameters.*

UNIT	MASS (KG)	FRACTION OF COSPIN TELEMETRY†	POWER (W)
SIM-1			5.1
AT	1.23	0.162	
LET	2.10	0.325	
DPU	1.69	0.030*	
SIM-2			2.6
HFT	0.33	0.035	
HET	4.49	0.393	
SIM-3 (A + B)			1.6
KET	2.45	0.055	
SIM-4	0.73	--	5.4
RTG Shield	1.60	--	--
TOTAL:	**14.6**	**1.000**	**14.7**

† COSPIN telemetry total = 5176 8-bit words per instrument data cycle (256 spacecraft frames)
* Contains spin counters, CPU status, and synch words

TABLE 3. *COSPIN LET detector summary.*

Detector	Type	Thickness (μm)	Thickness (mg/cm^2)	Area (cm^2)
D1	Ortec 600-30	32.2	7.503	6.0
D2	Ortec 600-100	95.9	22.345	6.0
D3	LBL 1000-2000	2054	478.6	10.0
D4	LBL 1250-2000	2000	466.0	12.5
D5	RCA C70102E	--	--	--

TABLE 4. *Low energy telescope data channels.*

Name	Logic	Primary Particle Type	Energy Range (MeV/n))	Geometric Factor (cm^2sr)	Avg. Time Resolution (sec)	Sectors	PHA Event Code
L1/P1	D1A $\overline{\text{D1B D2A D4 D5}}$	proton	0.9-1.2	9.1	32*	--	--
L2/P2	D1B $\overline{\text{D1C D2A D4 D5}}$	proton	1.2-3.0	9.1	32*	--	1
L3/P3	M2 $\overline{\text{I1}}$	proton†	1.8-3.8	0.58	32*	--	3
L4-L11/P3S	M2 $\overline{\text{I1}}$	proton†	1.8-3.8	0.58	32	8	--
L12/P4	M3 $\overline{\text{D2B D3B I5}}$	proton†	3.8-8.0	0.58	32*	--	4
L13-L20/P4S	M3 $\overline{\text{D2B D3B I5}}$	proton†	3.8-8.0	0.58	32	8	--
L21/P5	D2A D3B $\overline{\text{D1A D4}}$	proton	8.0-19.0	0.58	32*	--	5
L22/A1	D1C $\overline{\text{D2A D4 D5}}$	He	1.0-5.0	9.1	32*	--	2
L23/A2	D1A D2B I1 $\overline{\text{D3A D4 I2}}$	He†	1.9-3.7	0.58	32*	--	6
L24/A3	M3 I5 $\overline{\text{D3C I6}}$	He†	3.7-8.4	0.58	32*	--	7
L25/A4	D1A D2A D3C I5 $\overline{\text{D4 I6}}$	He†	8.4-19	0.58	32*	--	8
L26/H1	M2 I2 $\overline{\text{I3}}$	Li,Be,B†	1.9-4.9	0.58	128*	--	9
L27/H2	M3 I6 $\overline{\text{I7}}$	Li,Be,B†	4.9-26	0.58	128*	--	10
L28/H3	M2 I3 $\overline{\text{I4}}$	C,N,O†	2.6-7.1	0.58	128*	--	11
L29/H4	M3 I7 $\overline{\text{I8}}$	C,N,O†	7.1-39	0.58	128*	--	12
L30/H5	M2 I4	$Z \geq 10$†	3.0-9.0	0.58	128*	--	13
L31/H6	M3 I8 $\overline{\text{I9}}$	$10 \leq Z \leq 20$†	9.0-50	0.58	128*	--	14
L32/H7	M3 I9	$Z > 20$†	12-75	0.58	128*	--	15
L33/E1	D3A $\overline{\text{D1A D2A D4 D5}}$	electron	0.3-1**	--	128*	--	--
L34-L38/S1-S5	D1-D5 single detector counting rates	--	--	--	128*	--	--

M2 = D1A D2A $\overline{\text{D3A D4}}$
M3 = D1A D2A D3A $\overline{\text{D4}}$

Pulse Height Analysis (1 event per second at nominal bit rate)

D1 - D3	D1 - D3 total energy	1024 channels in each of two gain ranges
Flags	Discriminators/status	8 bits/event

* Rigid interval synchronized to telemetry format
† Particle identification by hyperbolic discriminator thresholds (I1-I9)
** Dominated by RTG-induced background in quiet times

TABLE 5. *Anisotropy telescopes data channels (identical channels defined for each telescope).*

Name	Logic	Primary Particle Type	Energy Range (MeV)	Geometric Factor (cm^2sr)	Avg. Time Resolution (s)	Sectors
A1	DA1 $\overline{\text{DA2 DB1 DC}}$	$Z \geq 1$	0.7-0.9	0.75	16	--
A2	DA2 $\overline{\text{DA3 DB1 DC}}$	$Z \geq 1$	0.9-1.3	0.75	16	--
A3	DA3 $\overline{\text{DA4 DB1 DC}}$	$Z \geq 1$	1.3-2.2	0.75	16	--
A4	DA1 DB1 $\overline{\text{DA4 DB2 DC}}$	proton	2.2-3.6	0.75	16	--
A5	DA1 $\overline{\text{DB2 DA4 DC}}$	proton	3.6-6.5	0.75	16	--
A38	DA4 $\overline{\text{DB1 DC}}$	$Z \geq 2$	3.1-7.2	0.75	128	--
A39	DA4 DB1 $\overline{\text{DB3 DC}}$	$Z \geq 2$	7.2-12	0.75	128	--
A40	DA4 DB3 $\overline{\text{DC}}$	$Z \geq 2$	12-23	0.75	128	--
A6-A13	A1 + A2	$Z \geq 1$	0.7-1.3	0.75	16	8
A14-A21	A3	$Z \geq 1$	1.3-2.2	0.75	64	8
A22-A29	A4	proton	2.2-3.6	0.75	64	8
A30-A37	A5	proton	3.6-6.5	0.75	64	8
A41-A44	A38	$Z \geq 2$	3.1-7.2	0.75	128	4
A45-A47	DA1, DB1, DC single detector counting rates	--	--	--	128	--

TABLE 6. *ULYSSES COSPIN – High energy telescope detectors and windows.*

Detector or Absorber	Sensitive Area (cm^2)	Total Thickness (μm)	Dead Layer (μm)	Sensitive Depth (μm)	Operating Bias (Volts)	Detector Manufacturer	Comment
Window 1	--	80	--	--	--	--	Kapton
Window 2	--	80	--	--	--	--	Phosphor/Bronze
D1	40	1194	69	1125	35	U. of Chicago	222 strip position sensing
Shield	--	12.7	--	--	--	--	Mylar/Al sandwich
D2	40	1194	67	1127	35	U. of Chicago	222 strip position sensing
Shield	--	12.7	--	--	--	--	Mylar/Al sandwich
D3	40	1194	68	1126	35	U. of Chicago	222 strip position sensing
D4	17	1194	65	1129	35	U. of Chicago	143 strip position sensing
Shield	--	12.7	--	--	--	--	Mylar/Al sandwich
D5	17	1194	61	1133	35	U. of Chicago	143 strip position sensing
Shield	--	12.7	--	--	--	--	Mylar/Al sandwich
D6	17	1219	65	1154	35	U. of Chicago	143 strip position sensing
Shield	--	12.7	--	--	--	--	Mylar/Al sandwich
K1	12	4986	24	4962	650	LBL	
K2	12	5041	23	5018	650	LBL	
K3	12	5049	20	5029	650	LBL	
K4	12	4853	25**	4828	650	LBL	
K5	12	4978	90**	4788	650	Kevex Corp.	
K6	12	5029	90**	4939	650	Kevex Corp.	
Shield	--	12.7	--	--	--	--	Mylar/Al sandwich
A	17	1067	170	897	35	U. of Chicago	

** No measurements available, values for similar detectors used

TABLE 7. *High energy telescope data channels.*

Name	Logic	Primary Particle Type	Energy Range (MeV(/n))	Geometric Factor (cm^2sr)	Avg. Time Resolution (s)	Sectors	PHA Priority
H1	D1 $\overline{D2}$ $\overline{D3}$ A $\overline{S}$	Proton	5.4-14	94	16	--	none
H2	D1M D2M $\overline{D3}$ D4 A $\overline{S}$ D1H	Proton	14-19	87	16	--	P3
H3	D1 D2 D4 $\overline{D6}$ A $\overline{S}$ (H)	Proton	24-31	16.2-14.9	16	--	P3
H4	D1 D2 D4 D6 K1 $\overline{K4}$ A $\overline{S}$ (H)	Proton	34-68	8.2-5.5	16	--	P2
H5	D1 D2 D4 K1 K4 A $\overline{S}$ (H)	Proton	68-92	5.2-3.6	16	--	P2
H6	D1 D2 $\overline{D1M}$ D3 D4 A $\overline{S}$	Electron	~1-3	87	16	--	P3
H7	D1 D2 D4 D6 K1 $\overline{D1M}$ $\overline{D2M}$ K4 A $\overline{S}$	Electron	~5-10	8.2-5.5	16	--	P2
H8	D1 D2 D4 $\overline{D1M}$ $\overline{D2M}$ D6 A $\overline{S}$	Electron	~3-5	16.2-14.9	16	--	P3
H9	D1 D2 D4 $\overline{K4}$ A $\overline{S}$ (H)	Proton	>92	3.6	16	--	P2
H10	D1H D2M D3 $\overline{D4}$ A $\overline{S}$	Z≥3	26-36 (^{12}C)	87	128	--	P2
H11	D1 D2 D4 (H) $\overline{K4}$ A $\overline{S}$	Z≥3	44-127 (^{12}C)	16.2-5.5	128	--	P1
H12	D1 D2 D4 K4 (H) A $\overline{S}$	Z≥3	127-173 (^{12}C)	5.2-3.6	128	--	P1
H13	D1 D2 D4 K4 (H) A $\overline{S}$	Z≥3	>173 (^{12}C)	3.6	64	--	P1
H45S	D1 D2 D4 D6 K1 A $\overline{S}$ (H)	Proton	34-92	8.2-3.6	128	8	P2
H7S	D1 D2 D4 D6 K1 $\overline{D1M}$ $\overline{D2M}$ K4 A $\overline{S}$	Electron	~5-10	8.2-5.5	128	8	P2
H14 - H19	D1 - D6 Single Detector Rates	--	--	--	128	--	--
H20 - H25	K1 - K6 Single Detector Rates	--	--	--	128	--	--
H26, H27	A, S Single Detector Rates	--	--	--	128	--	--

(H) = (D5H + D6H + K1H + K2H + K3H + K4H + K5H) where + ==> inclusive or

Pulse Height Analysis (Avg. 5.33 seconds per event at nominal bit rates)

Name	Measures	Description
P1-P6	D1 - D6 position	4096 channels in each of two gain ranges
E1-E6	D1 - D6 total energy	" " " " " " " "
K1-K6	K1 - K6 total energy	" " " " " " " "
Flags	Discriminators, sectors, status	64 bits per event

PHA Priorities (Normal Mode)

P1:	D1 D2 D4 (H) $\overline{A}$ $\overline{S}$	
P2:	D1H D2 A $\overline{S}$ + D1 D2 D6 $\overline{A}$ $\overline{S}$ + D1 D2 D4 (H) $\overline{S}$	+ ==> inclusive or
P3:	D1M D2M $\overline{A}$ $\overline{S}$ + D1 D2 D4 G	G is true during alternate spacecraft formats

TABLE 8. *HET commands.*

Command		Effect on Logic
C1		Replace D1 by D3
C2		Replace D2 by D3, remove D2 from H6
C3		Remove D3
C4		Replace D4 by D5, except in P2b, H3,4,7, and 8
C5		Add K1 to D4D6 terms
C6		Replace K1 by K2
C7		Replace K4 by K3
C8		Replace A by K6
C9		Turn off S high voltage
C10		Replace D2 by D2M in P2a, $\overline{D2}$ by D2M in H1
C11		Replace (H) by D2H
C12		Initiate Calibrate Mode
C13	(C5+C6)	Turn off K1-K3 HV bias
C14	(C6+C7)	Turn off K4-K6 HV bias
C15	(C5+C7)	Turn off K1-K6 HV bias
C16	(C5+C6+C7)	Turn off In-Flight Calibrator
C17-C23	(Various Combinations of C1, C4-C7, C10)	Heater Control Commands

TABLE 9. *High flux telescope data channels.*

Name	Discriminator Discriminator Level	Primary Particle Type	Energy Range* (MeV(/n))	Species for Energy Range	Geometric Factor (cm^2sr)	Avg. Time Resolution (s)	Sectors
F1†	J0	Z≥1	0.28-7.0	Protons	0.033	16/readout 256 for same disc. level	--
	J1	Z≥1	0.50-2.27	Protons			
	J2	Z≥1	0.76-1.37	Protons			
	J4	Z≥2	0.36-3.9	Helium			
	J6	Z≥2	0.51-2.26	Helium			
	J8	Z≥2	0.64-1.66	Helium			
	J10	Z≥2	0.78-1.35	Helium			
F2	Lo	Z≥1	0.29-6.7	Protons	0.033	16	--
	Hi	Z≥1	0.55-1.95	Protons			
F2s	[same as for F2]					32	8 sampled from 32
						128	32
F3		Z≥2	0.68-1.56	Helium	0.033	32	--
F4		Z≥3	0.8-4.9	Carbon	0.033	64	--
F5		Z≥12	0.8-34†	Iron	0.033	64	--

† F1 steps through 16 discriminator levels in sequence in standard flight mode
* Energy ranges from range-energy relations

TABLE 10. *Electron telescope data channels.*

Name	Logic	Primary Particle Type	Energy Range (MeV(/n))	Geometric Factor (cm^2sr)	Avg. Time Resolution (s)	Sectors	PHA
K1 (P1)	D11 $\overline{D12\,C10\,D20\,C20\,S20\,A0}$	proton	2.7-5.4	6.5	128	--	--
K21-28 (P4)	D12 $\overline{D13\,C10\,D20\,C20\,S20\,A0}$	proton	5.4-23.1	6.5	128	8	--
K3 (P32)	D11 D20 $\overline{D12\,C10\,C20\,S20\,A0}$	proton	34.1-125	0.72	128	--	P1
K34 (P116)	D10 D20 S20 $\overline{D12\,C10\,C20\,A0}$	proton	125-320	1.2	128	--	P1
K12 (P190)	D10 D20 C20 S20 $\overline{D11\,C10\,D21\,C21\,A0}$	proton	320-2100	1.7	128	--	P0
K10 (P4000)	D10 C10 D20 C20 S20 $\overline{D11\,C11\,D21\,C21\,A0}$	proton	>2100	1.7	128	--	P0
K2 (A4)	D13 $\overline{C10\,D20\,C20\,S20\,A0}$	He	6.0-20.4	6.5	128	--	--
K33 (A32)	D12 D21 $\overline{D13\,C10\,C20\,S20\,A0}$	He	34.2-125	0.72	128	--	P1
K29 (A116)	D12 D21 S20 $\overline{D13\,C10\,C20\,A0}$	He	125-320	1.0	128	--	P1
K31 (A190)	D11 D21 C20 S20 $\overline{D12\,C10\,A0}$	He	320-2100	1.4	128	--	P0
K30 (A4000)	D11 C10 D21 C20 S20 $\overline{D12\,C11\,A0}$	He	>2100	1.4	128	--	P1
K13-20 (E4)	D10 C10 D20 $\overline{D11\,C11\,D21\,C20\,S20\,A0}$	electron	2.5-7	0.26	128	8	P1
K11 (E12)	D10 C10 D20 C20 $\overline{D11\,C11\,D21\,S20\,A0}$	electron	7-170	0.40	128	--	P3
K32 (E300)	D10 C10 D20 C21 S20 $\overline{D11\,C11\,D21}$ (A0+A1)	electron	>170	0.38	128	--	P2

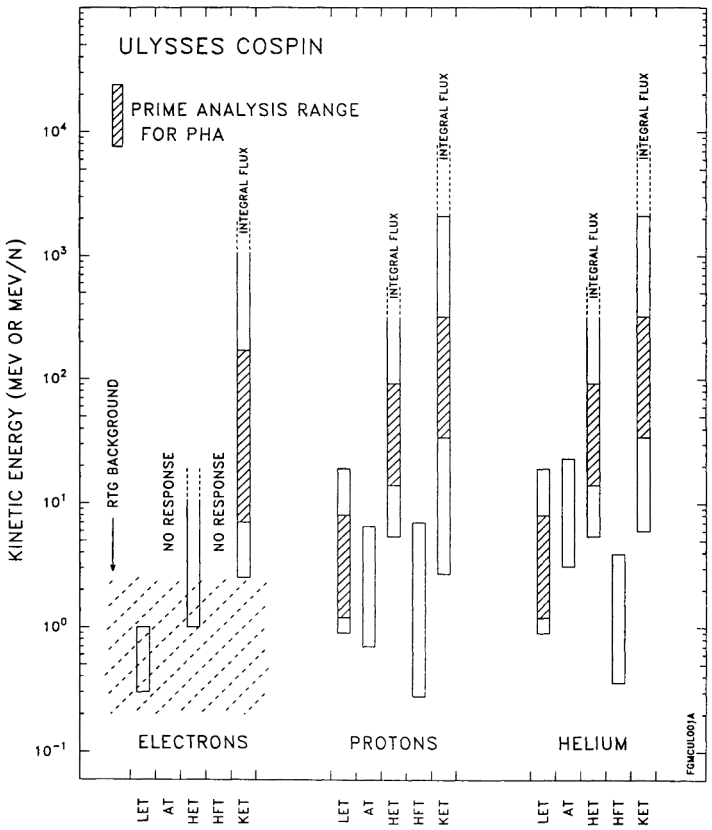

FIGURE 1. Electron, proton and helium energy ranges of the COSPIN sensor subsystems. Shading indicates the energy range for which background from the RTG's contributes to the electron measurements.

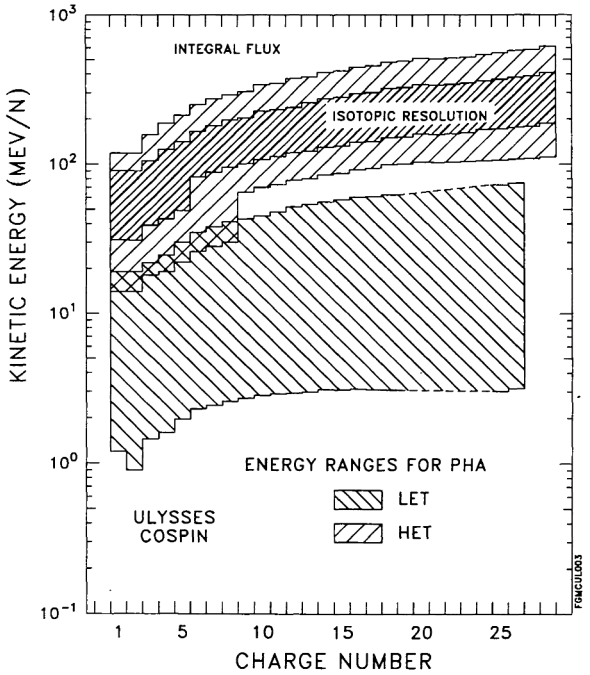

FIGURE 2. Energy and nuclear charge ranges of the HET and LET COSPIN sensor subsystems.

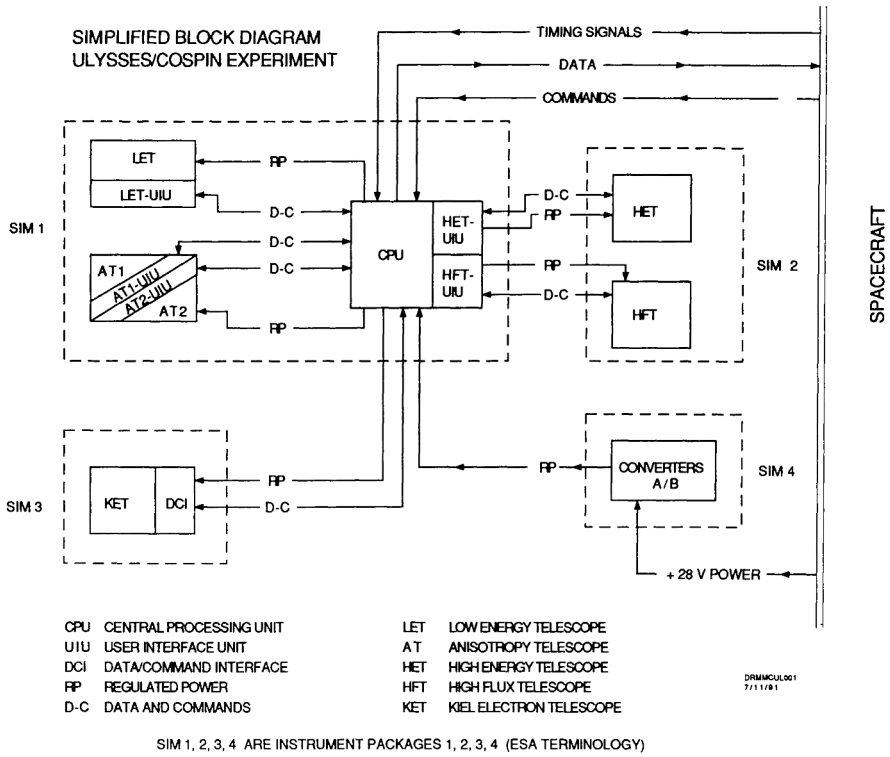

FIGURE 3. Simplified block diagram of the COSPIN Experiment.

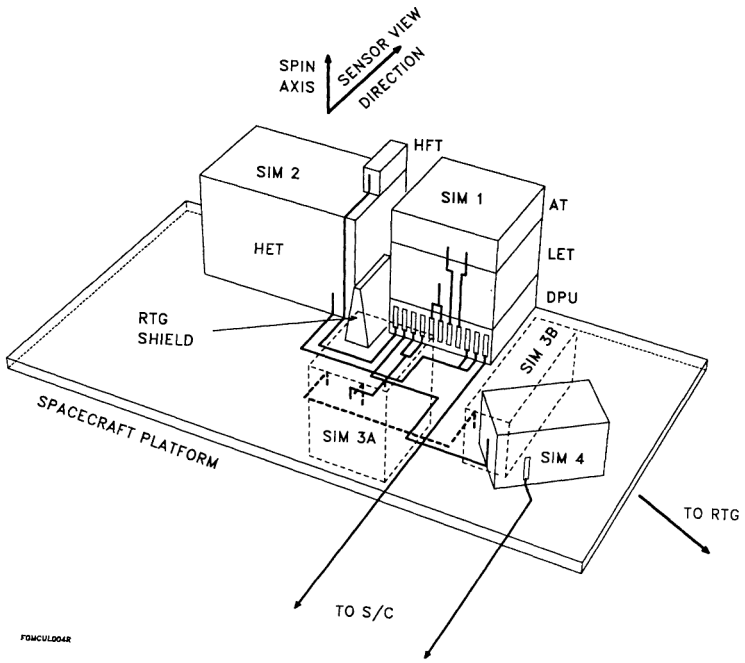

FIGURE 4. Schematic diagram showing the five COSPIN instrumentation packages and their interconnections as mounted on the Ulysses spacecraft platform, viewed from inside the spacecraft. Dotted lines indicate instrumentation mounted on the under-side of the platform.

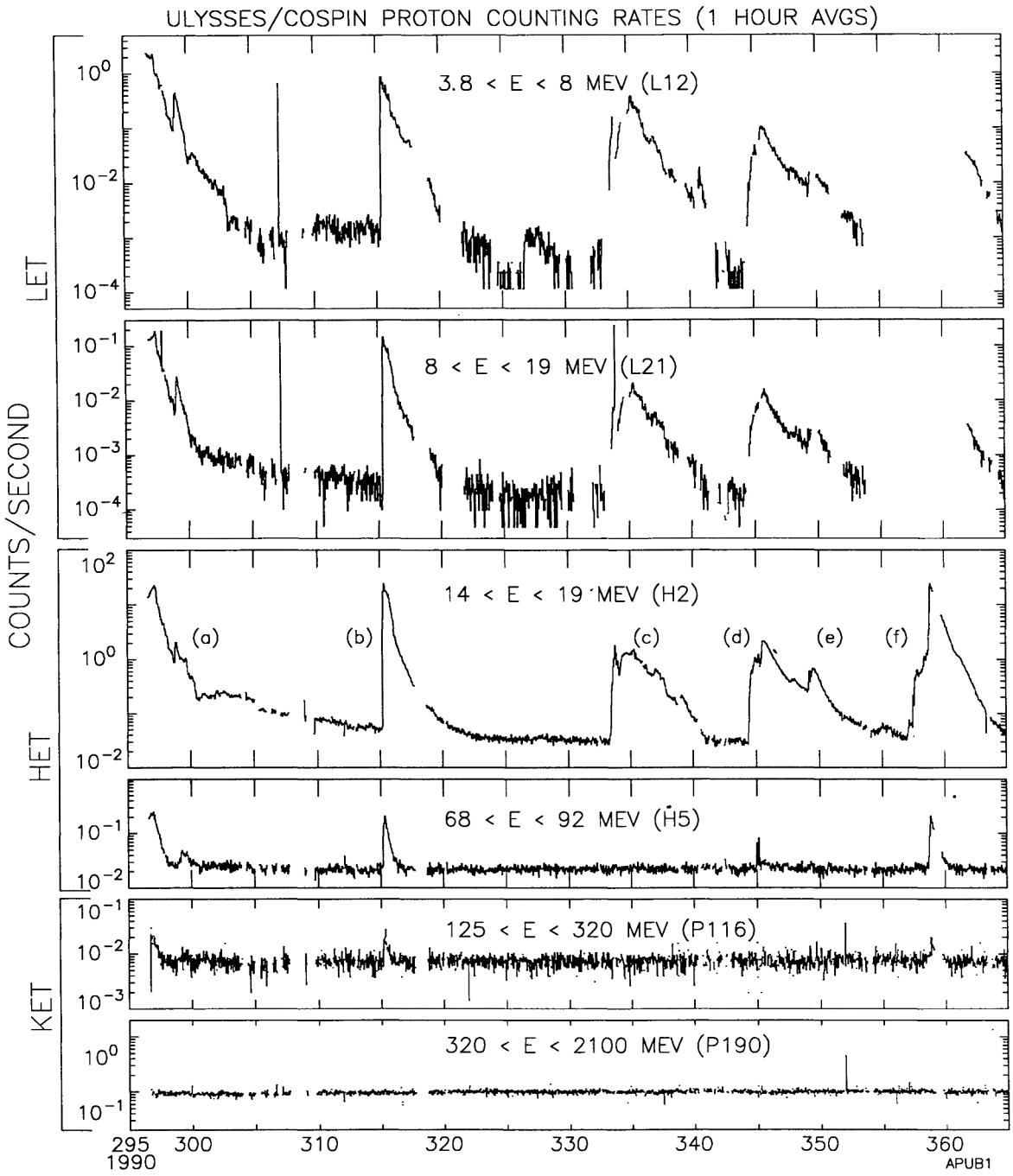

FIGURE 5. Proton counting rates (counts s^{-1}) with one hour averages for the first 70 days of the Ulysses Mission following COSPIN instrument turn-on. For identification of the data channels see Tables 4, 7, and 10.

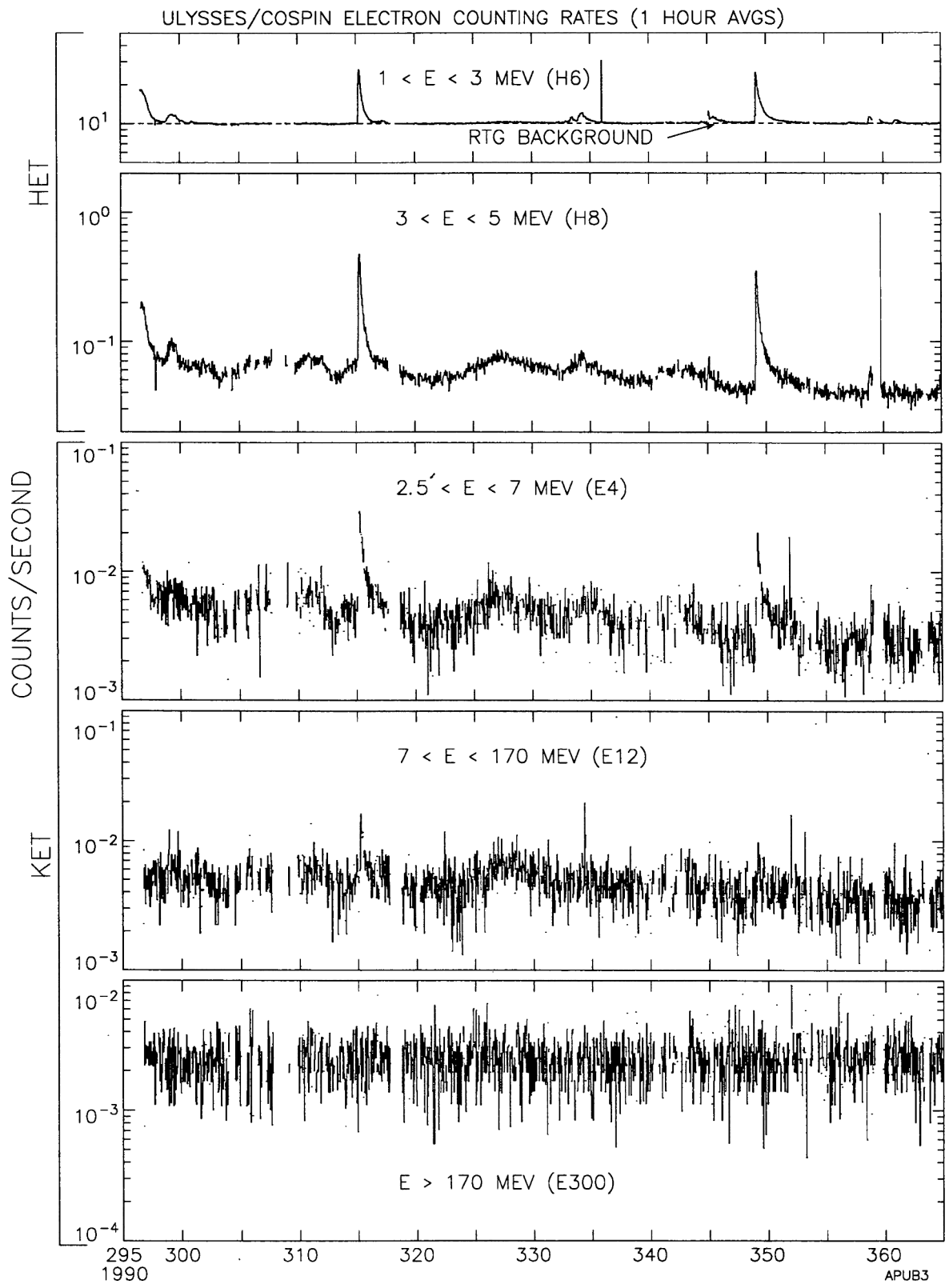

FIGURE 6. Electron counting rates (counts s^{-1}) with one hour averages for the first 70 days of the Ulysses Mission following COSPIN turn-on.

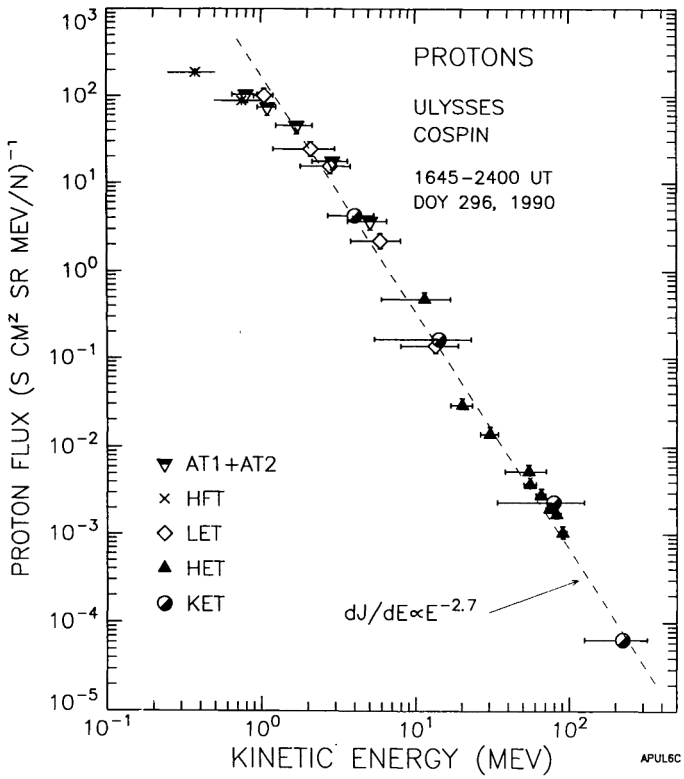

FIGURE 7. The differential energy spectrum of solar flare protons from the solar particle event in progress on Day 296 when COSPIN power was turned on (cf. Fig. 5). The spectrum is $\propto E^{-2.7}$ above ~ 2 MeV.

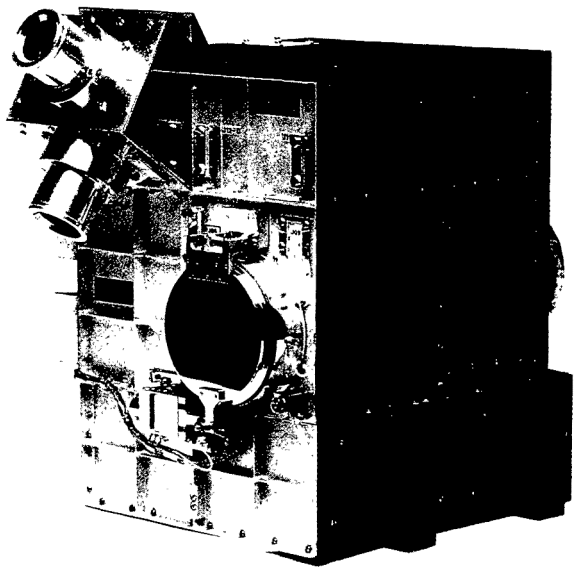

FIGURE 8. Photograph of the SIM-1 unit of COSPIN. The LET is mounted below the twin AT telescopes.

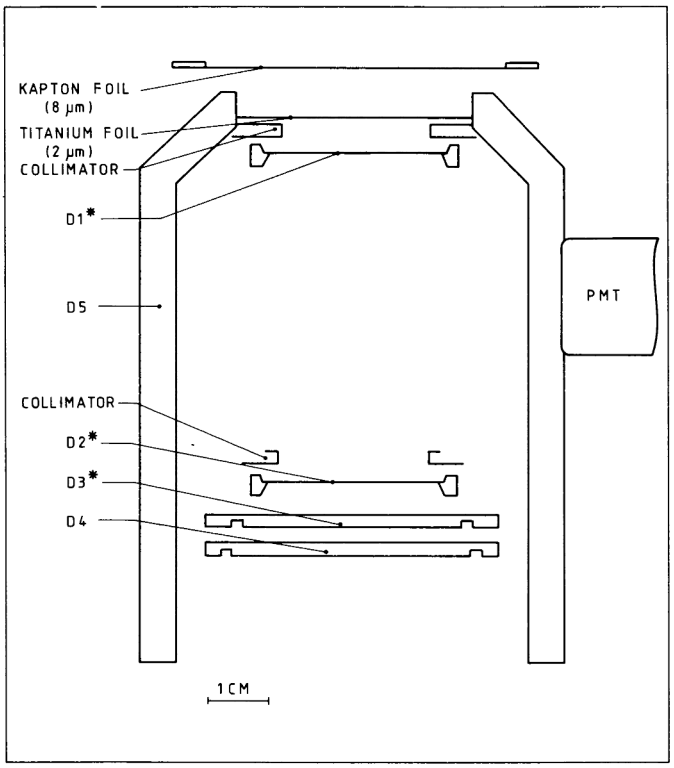

FIGURE 9. Schematic representation of the LET detector telescope. D_n^* denotes a pulse height analyzed detector.

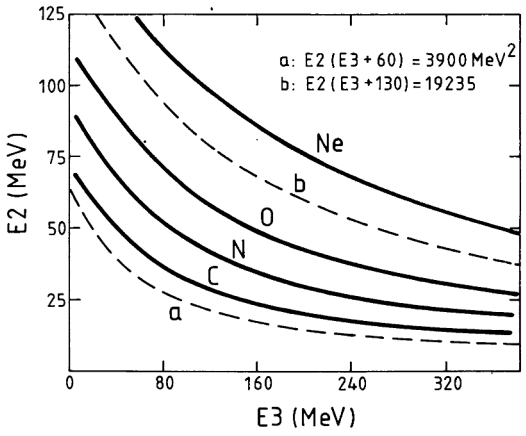

FIGURE 10. LET Particle Identifier (PI) boundaries (dashed lines) for CNO group events stopping in D_3.

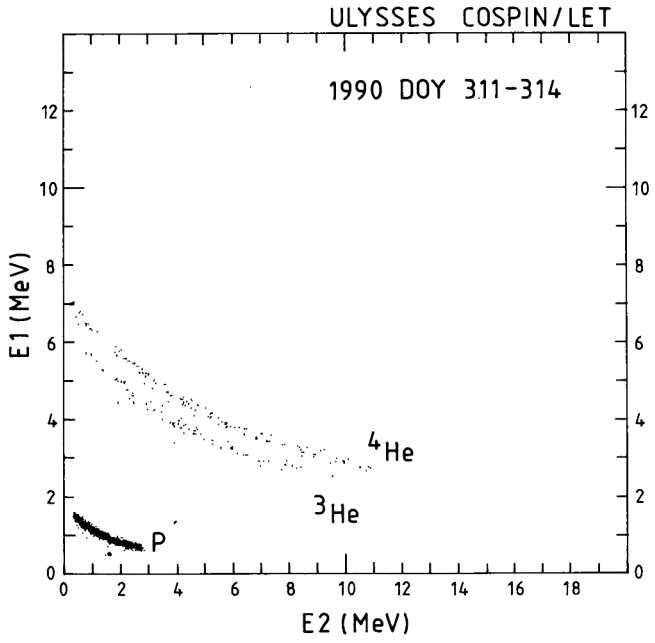

FIGURE 11. Flight data from the COSPIN LET. Shown is the D_1 vs. D_2 pulse height matrix for the ^{3}He-rich period 7-10 November, 1990.

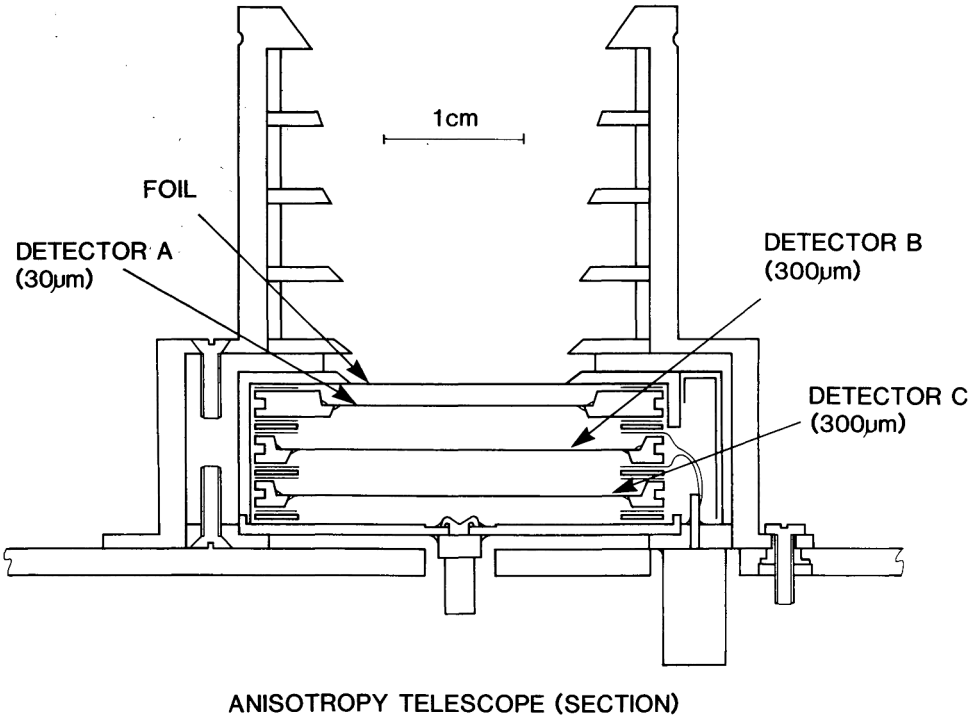

FIGURE 12. Schematic cross-section of the AT telescope. COSPIN includes two identical AT telescopes with axes at angles of 60° and 145° to the spacecraft spin axis.

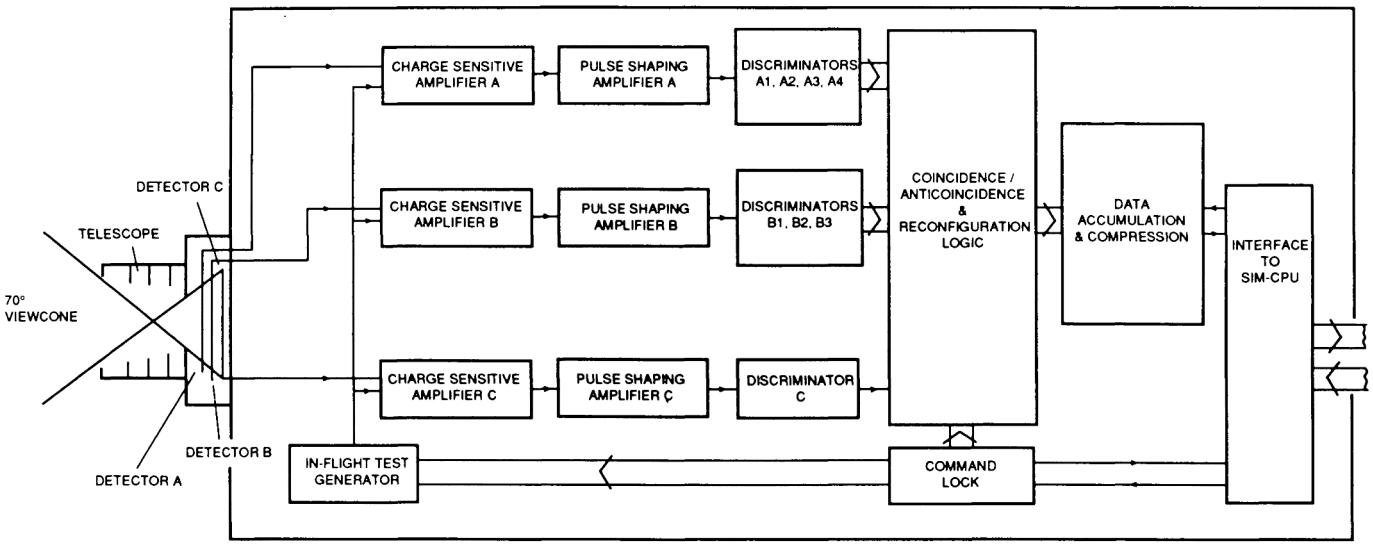

FIGURE 13. Functional block diagram of the AT telescope electronics.

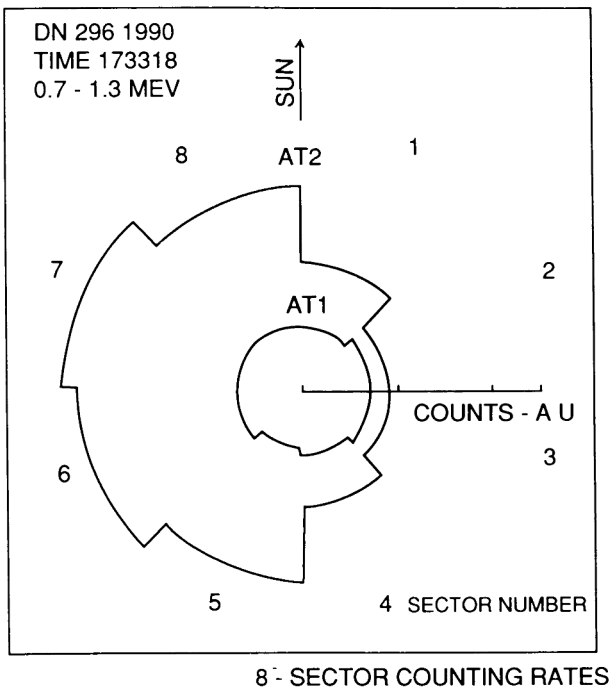

FIGURE 14. Anisotropies measured by AT-1 and AT-2. The counting rates are shown in arbitrary units (A U), normalized to the maximum counting rate observed in the AT2 telescope.

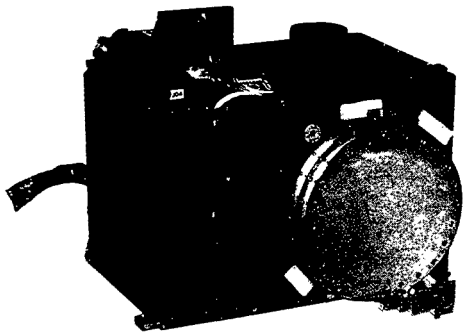

FIGURE 15. Photograph of SIM-2 showing the HET with the HFT mounted on top. The covers for the HET and HFT apertures, shown here in the closed position, were opened by telecommand after launch.

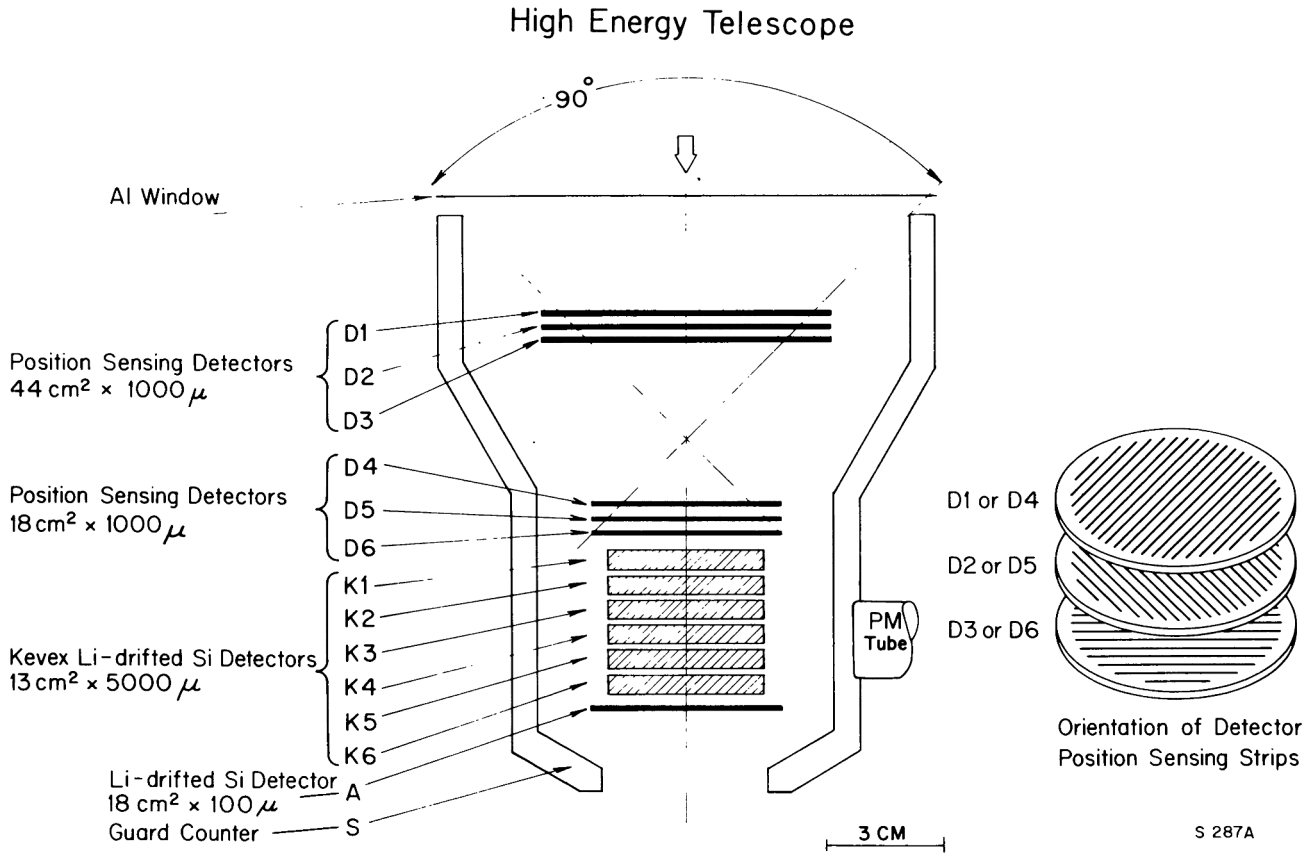

FIGURE 16. Schematic cross section of the High Energy Telescope.

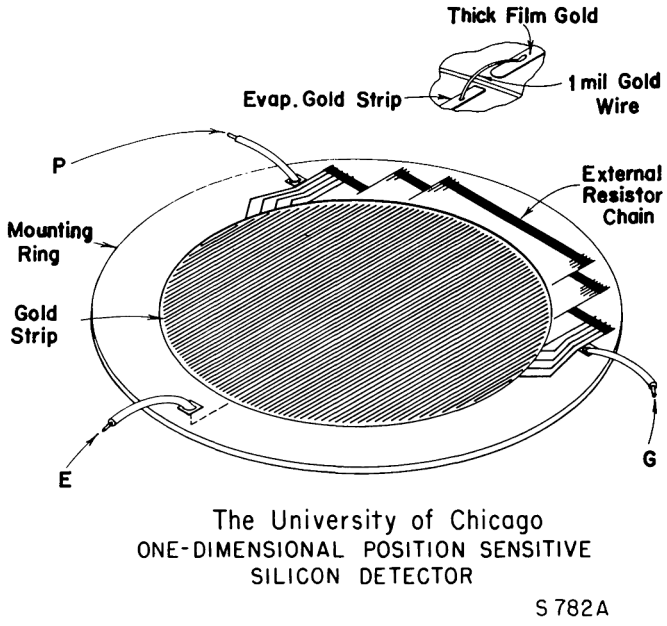

FIGURE 17. Schematic diagram of a position sensing detector of the type used for the HET detectors $D_1 - D_6$.

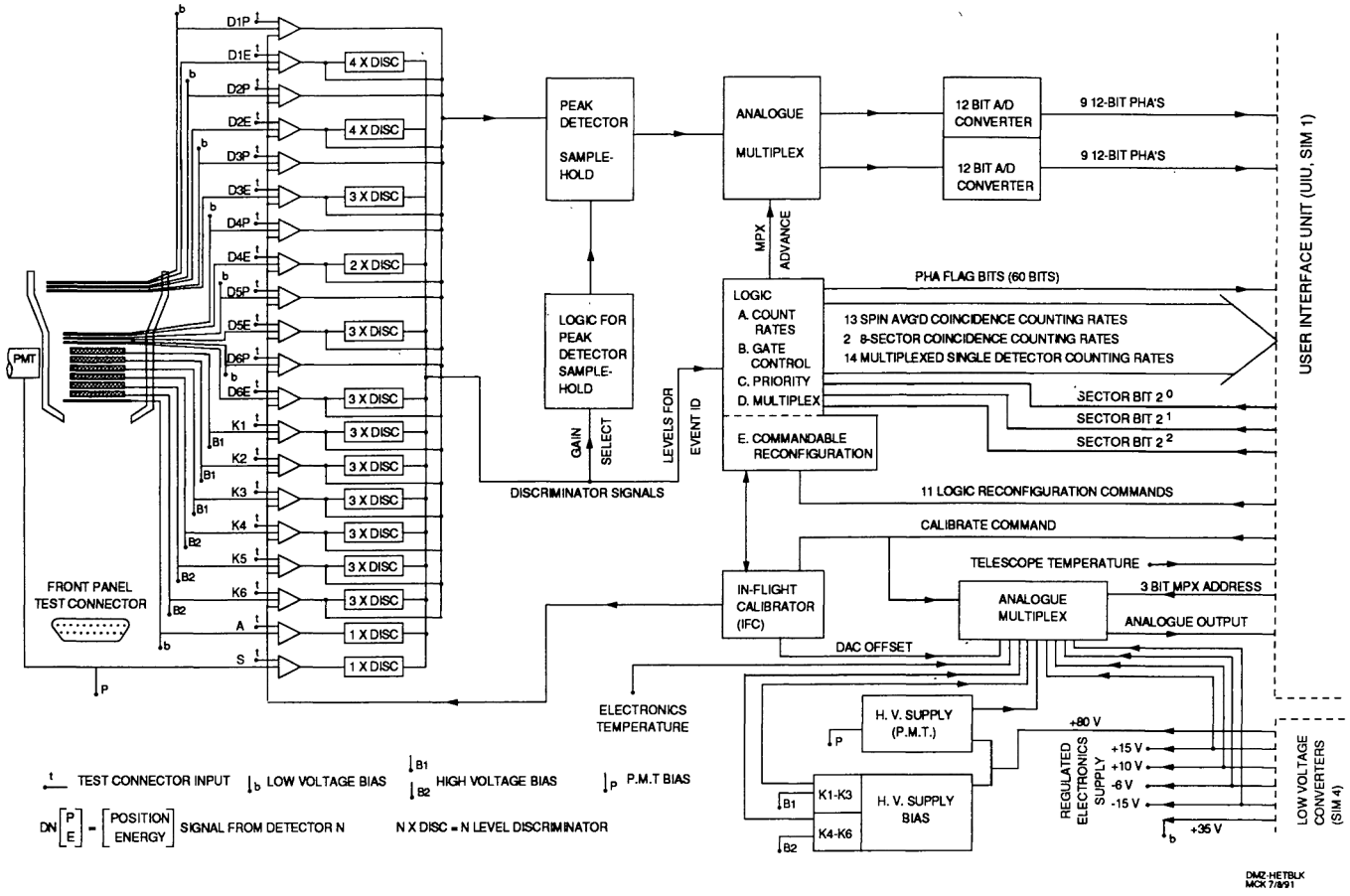

FIGURE 18. Functional block diagram of the HET electronics.

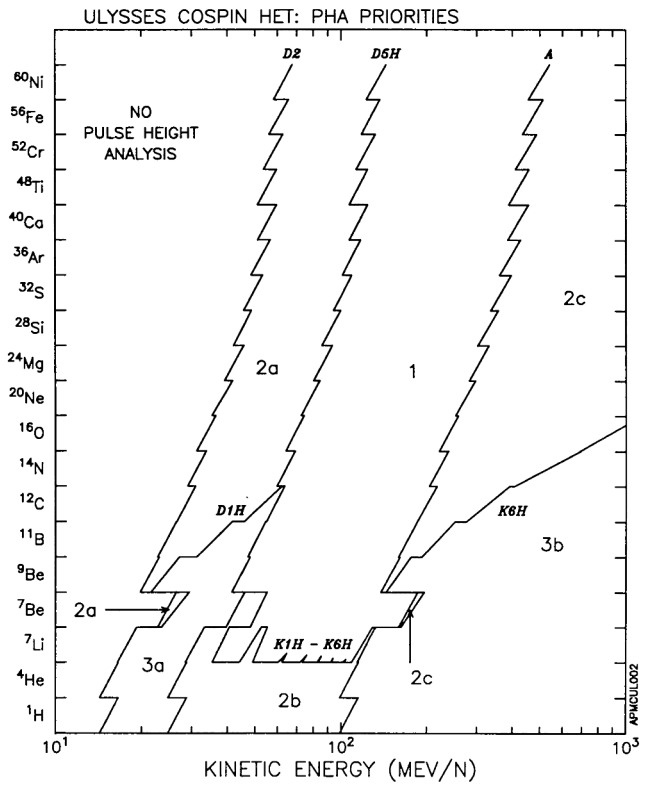

FIGURE 19. Energy ranges for HET PHA priorities 1, 2, and 3 as a function of particle charge, Z

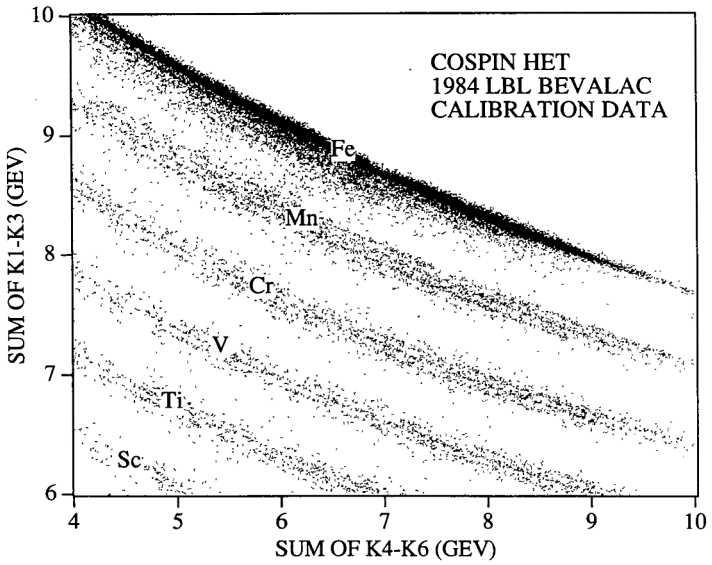

FIGURE 20. dE/dX vs. E matrix from the HET obtained for sub-iron nuclei during an accelerator calibration at the Lawrence Berkeley Laboratory Bevalac.

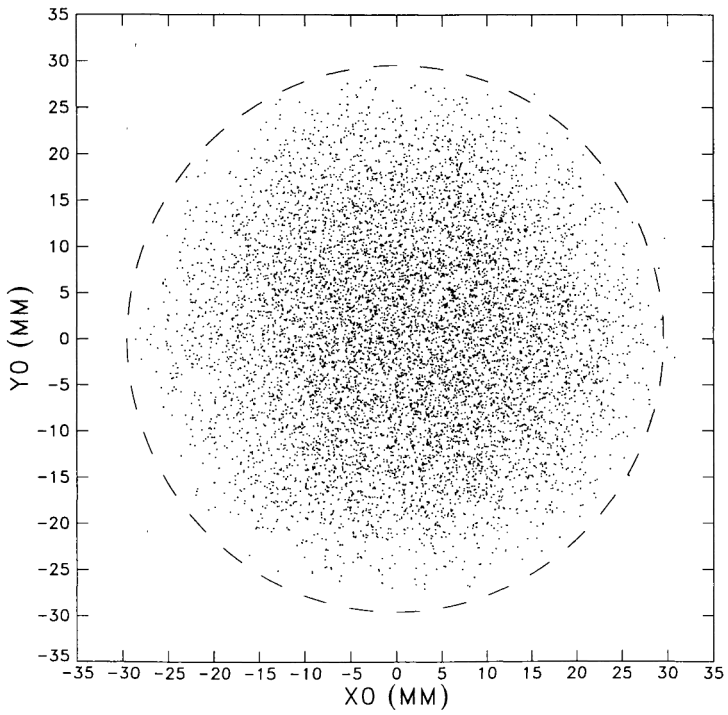

FIGURE 21. Location of particle trajectories at a plane midway between the detectors D_3 and D_4 computed from position measurements by detectors $D_1 - D_6$ for particles with calculated charge, Z, greater than 1.5. 118 days of post-launch data are included in this figure. The dashed circle indicates the boundary of the region allowed by geometry of the telescope for particles passing through D_3 and D_4.

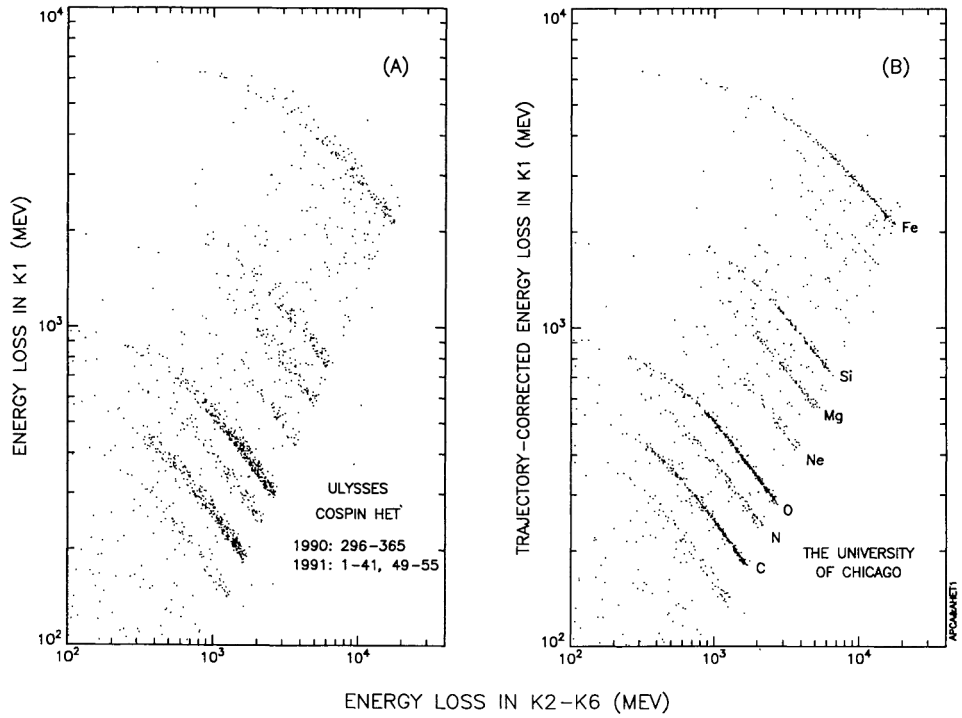

FIGURE 22. a,b) HET dE/dX vs. E matrices from the HET for particles stopping in detectors $K_2 - K_6$ for in-flight data before (a) and after (b) correction for angle based on trajectory information from detectors $D_1 - D_6$.

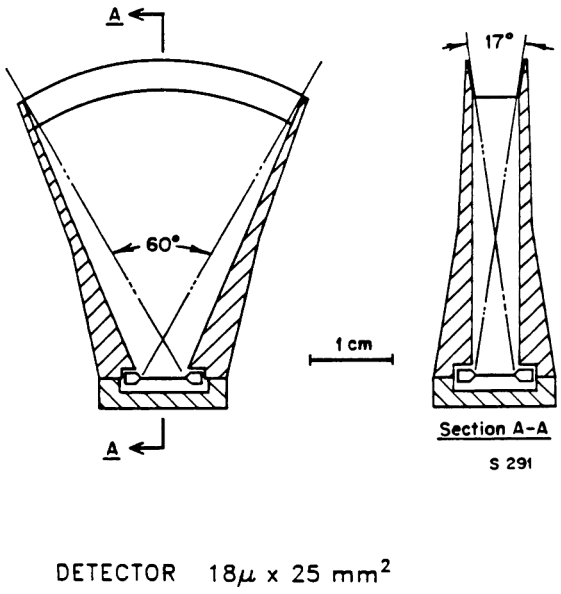

FIGURE 23. Schematic cross-section of the High Flux Telescope (HFT).

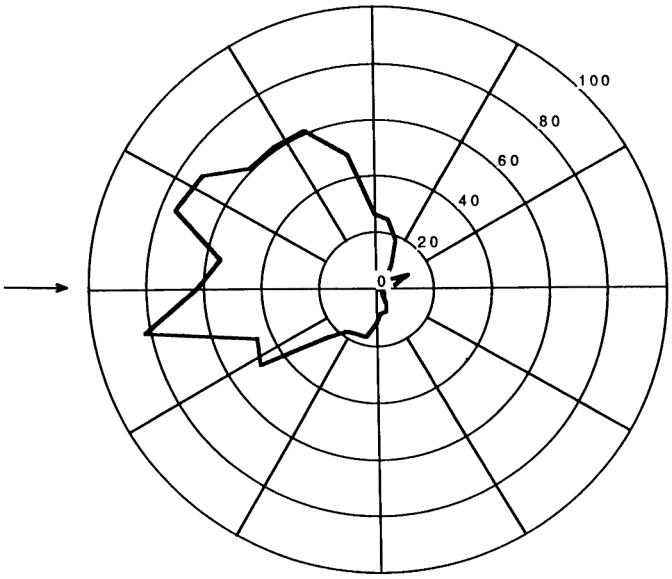

FIGURE 24. Flux of 0.29 - 6.7 MeV protons $\left(\mathrm{s\ cm^2\ sr}\right)^{-1}$ versus the mean angle of Ulysses $+XZ$ reference plane with respect to Sun crossing derived from the F_2 sectored counting rate. The arrow indicates the angle at which particles flowing from the sun along the mean interplanetary magnetic field would be expected to appear. Data are from 0:54:11 to 1:45:23 UT, January 3, 1991, approximately one week after first opposition, when Ulysses was 0.63 AU from Earth.

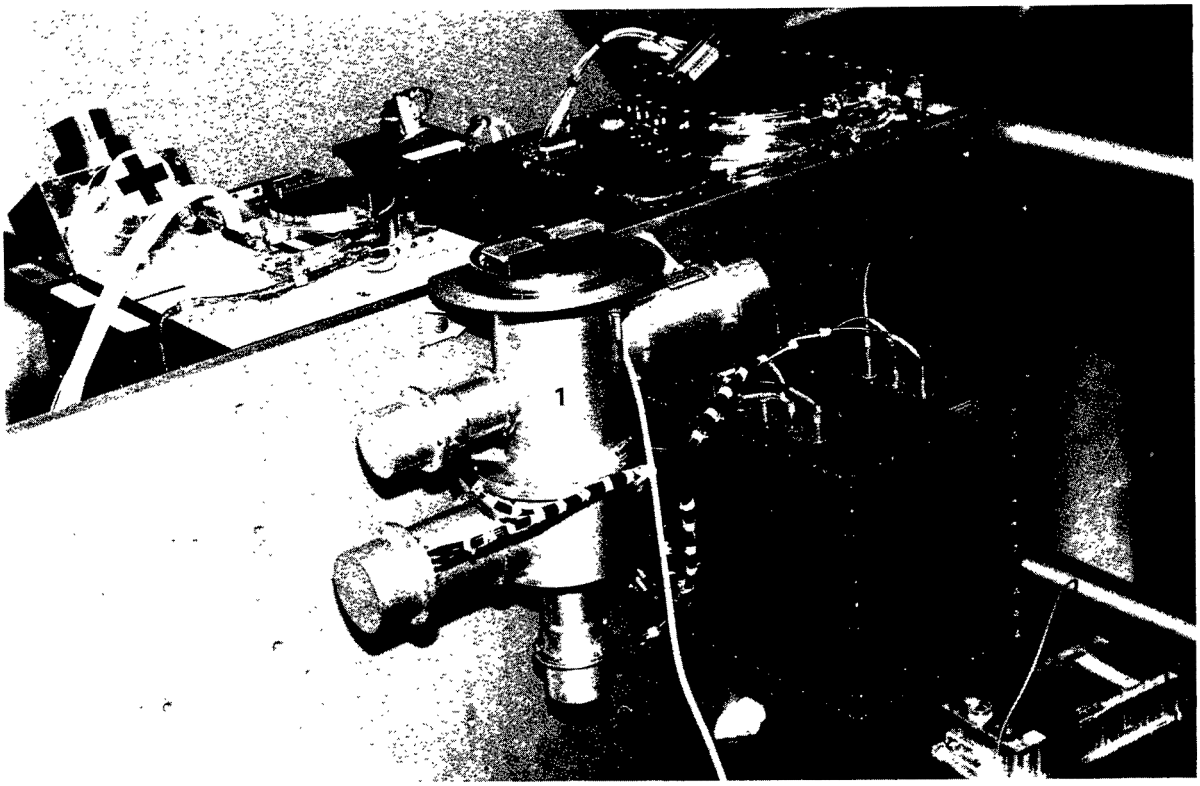

FIGURE 25. Photograph of the SIM-3 units. SIM3A contains the digital and analogue electronics for the Kiel Electron Telescope (KET), while SIM3B consists of the sensors for the KET.

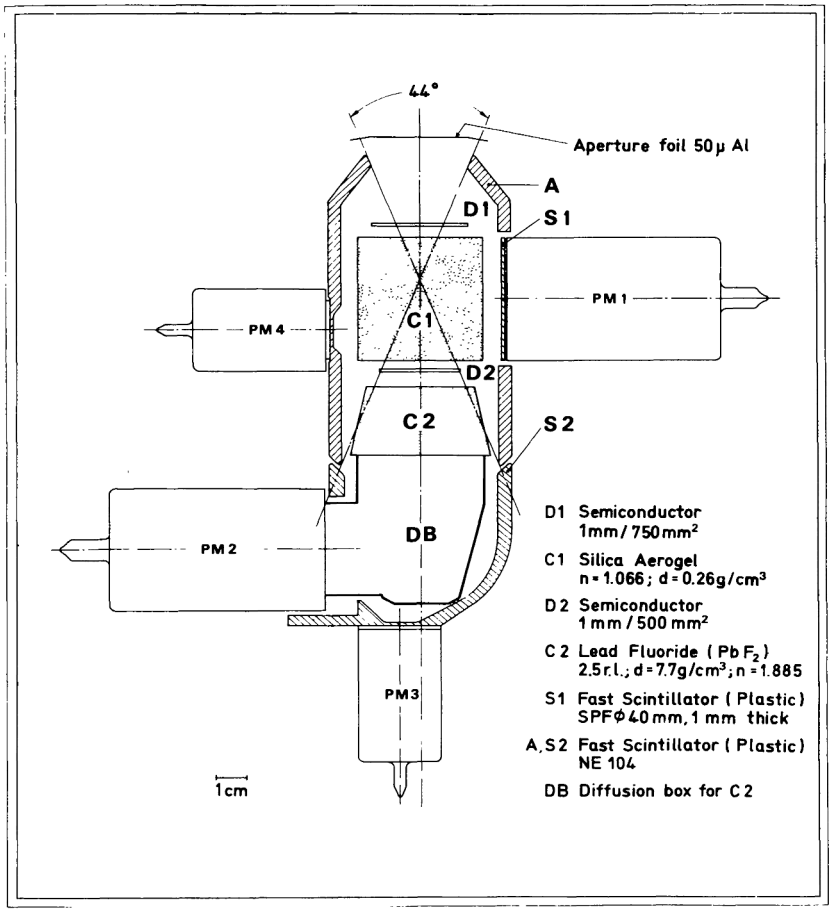

FIGURE 26. Schematic cross-section of the KET telescope.

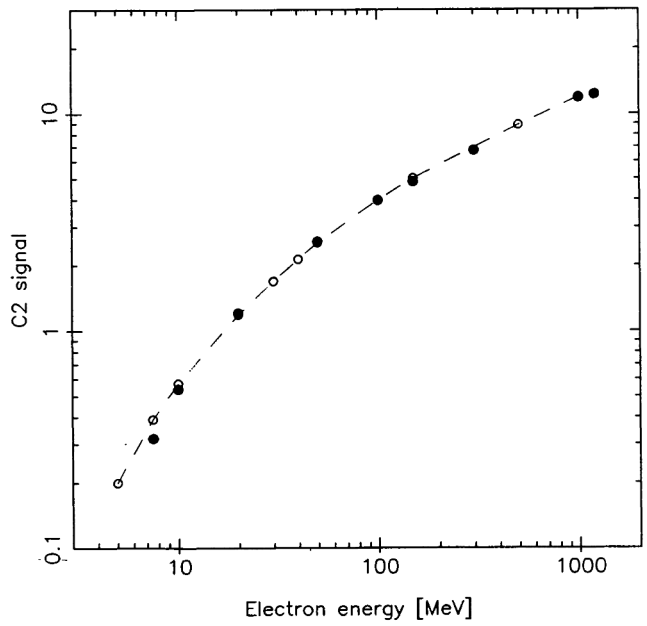

FIGURE 27. Average value of the calorimeter signal (arbitrary units) as a function of the incident electron energy. Full circles: accelerator measurements; open circles: simulation results.

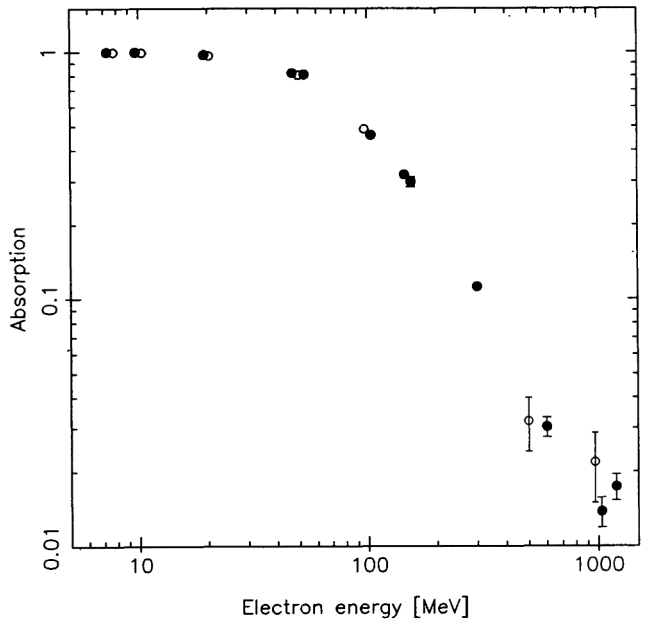

FIGURE 28. Variation of the absorption with the electron energy. The absorption is defined as the ratio of $E_4 + E_{12}$ events to $E_4 + E_{12} + E_{300} + P_{4000}$ events. Full circles: accelerator measurements; open circles: simulation results.

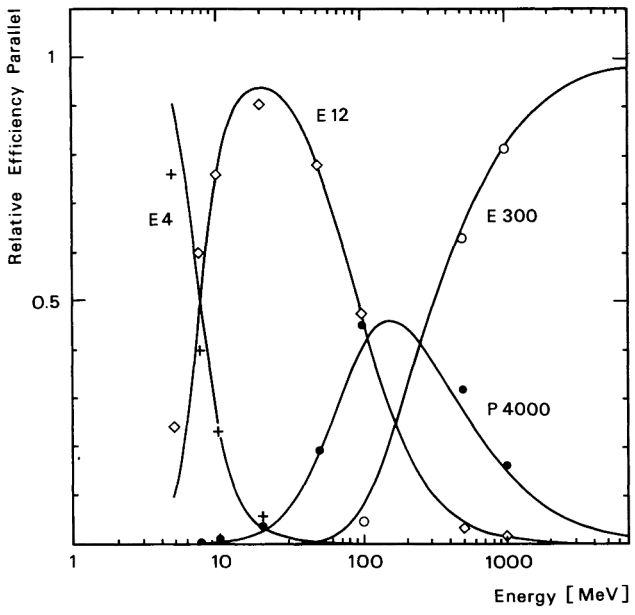

FIGURE 29. Relative efficiencies of the electron sensitive channels E_4, E_{12}, E_{300}, and P_{4000}, for an axially incident electron beam. The full lines are fits to the accelerator measurements; the symbols are simulation results (cross: E_4, open diamond: E_{12}, open circle: E_{300}, full circle; P_{4000}).

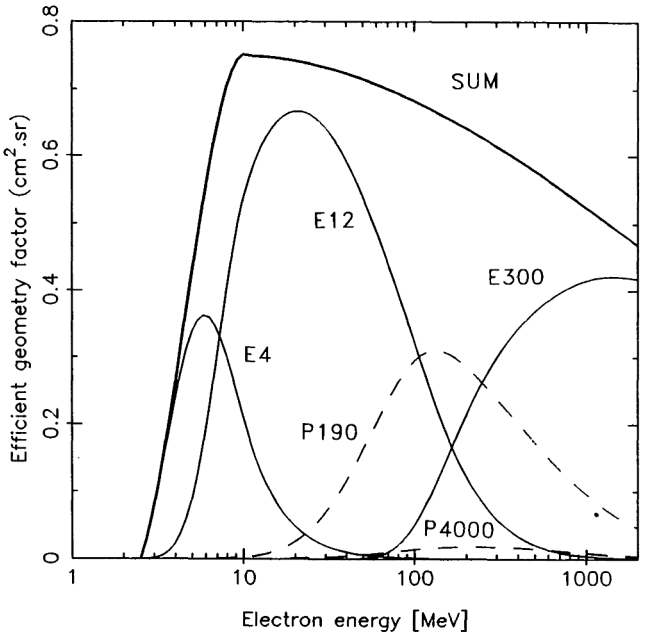

FIGURE 30. Effective geometry factors of each electron sensitive channel as a function of the electron energy, for an isotropic flux. Full thin lines from left to right: effective geometry factor for E_4, E_{12}, and E_{300}. Dashed lines: effective geometry factor for electron induced P_{190} (lowest) and P_{4000} (highest). Full thick line: sum.

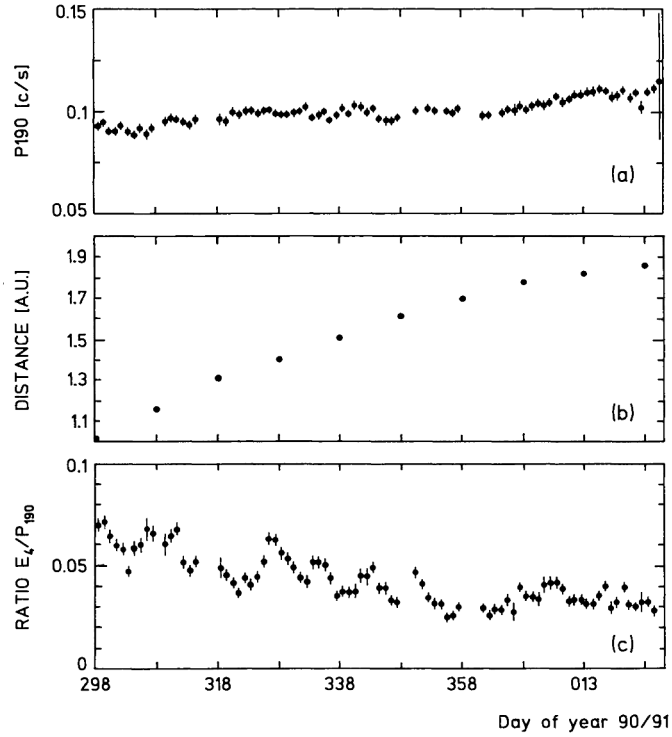

FIGURE 31. a) KET high energy proton counting rate P190 (320-2200 MeV), showing decreasing modulation. b) Shortest distance from Jupiter to the magnetic field line connected to Ulysses for an assumed solar wind speed of 400 km/s. c) Low energy electron to high energy proton flux ratio E_4/P_{190} as detected by the KET, suggesting a Jovian origin of electrons.

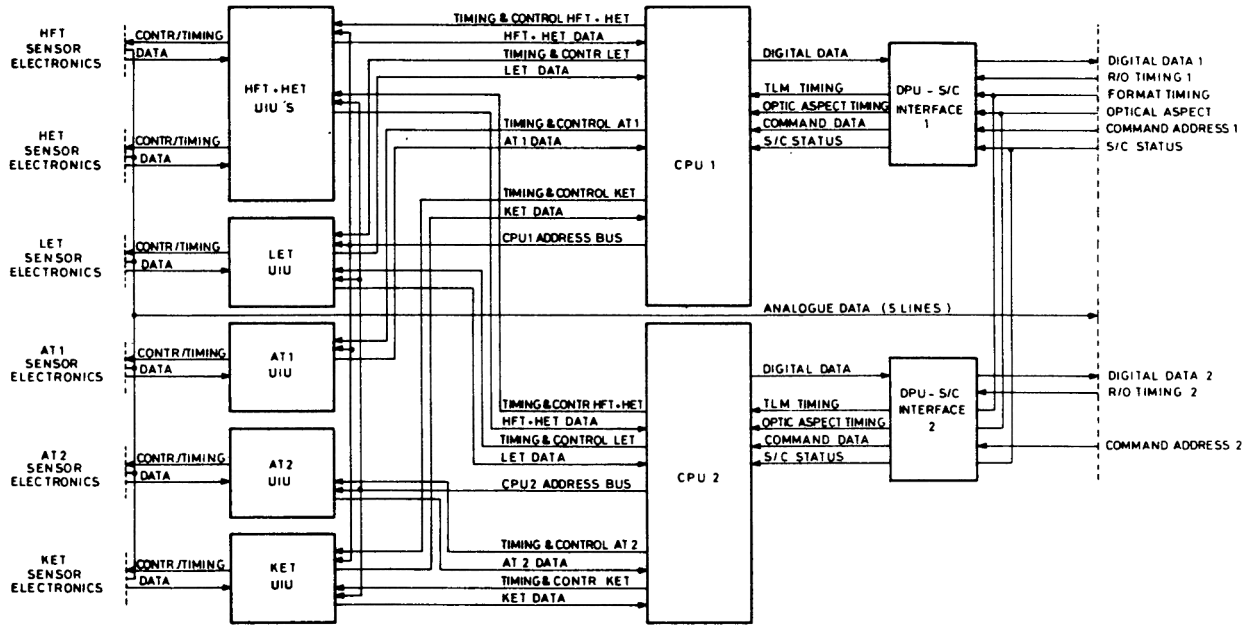

FIGURE 32. DPU functional block diagram.